



HHS Public Access

Author manuscript

Nat Immunol. Author manuscript; available in PMC 2019 August 18.

Published in final edited form as:

Nat Immunol. 2019 March ; 20(3): 337–349. doi:10.1038/s41590-018-0311-z.

The transcription factor c-Myb regulates CD8⁺ T cell stemness and antitumor immunity

Sanjivan Gautam¹, Jessica Fioravanti¹, Wei Zhu², John B. Le Gall¹, Philip Brohawn³, Neal E. Lacey¹, Jinhui Hu¹, James D. Hocker¹, Nga Voong Hawk¹, Veena Kapoor¹, William G. Telford¹, Devikala Gurusamy⁴, Zhiya Yu⁴, Avinash Bhandoola⁵, Hai-Hui Xue⁶, Rahul Roychoudhuri⁷, Brandon W. Higgs³, Nicholas P. Restifo⁴, Timothy P. Bender^{8,9}, Yun Ji^{1,10}, and Luca Gattinoni¹

¹Experimental Transplantation and Immunology Branch, Center for Cancer Research, National Cancer Institute, Bethesda, MD 20892, USA

²Department of Bioinformatics, Inova Translational Medicine Institute, Fairfax, VA 22031, USA

³MedImmune, 1 Medimmune Way, Gaithersburg, MD 20878, USA

⁴Surgery Branch, Center for Cancer Research, National Cancer Institute, Bethesda, MD 20892, USA

⁵Laboratory of Genome Integrity, Center for Cancer Research, National Cancer Institute, Bethesda, MD 20892, USA

⁶Department of Microbiology, Carver College of Medicine, University of Iowa, Iowa City, IA 52242, USA

⁷Laboratory of Lymphocyte Signaling and Development, Babraham Institute, Cambridge, UK

⁸Department of Microbiology, University of Virginia, Charlottesville, VA 22908, USA

⁹Beirne B. Carter Center for Immunology Research, University of Virginia, Charlottesville, VA 22908, USA

¹⁰Current affiliation: Cellular Biomedicine Group (CBMG), Gaithersburg, MD 20874

Users may view, print, copy, and download text and data-mine the content in such documents, for the purposes of academic research, subject always to the full Conditions of use:http://www.nature.com/authors/editorial_policies/license.html#terms

Correspondence should be addressed to L.G. (gattinol@mail.nih.gov), Center for Cancer Research, National Cancer Institute, Building 10 - CRC, Room 3E-3150, Bethesda, MD 20892, USA. Tel: +1-240-760-6165.

AUTHOR CONTRIBUTIONS

S.G., J.F., J.B.L., P.B., N.E.L., J.H., J.D.H., N.V.H., V.K., W.G.T., D.G., R.R. and Y.J. performed experiments; S.G., W.Z., J.B.L., Y.J. and L.G. analyzed experiments; S.G., B.W.H., R.R., N.P.R., T.P.B. and L.G. designed experiments; Z.Y., H.H.X., A.B. and T.P.B. contributed reagents; W.Z., J.B.L., R.R., N.P.R., T.P.B. and Y.J. edited the manuscript; S.G. and L.G. wrote the manuscript.

COMPETING FINANCIAL INTERESTS

P.B. and B.W.H. are full-time employees of MedImmune and have stock in AstraZeneca. S.G., Y.J. and L.G. have a pending patent on c-Myb technology. Other authors have no competing interests.

ACCESSION CODES

RNA-seq data are deposited to the Gene Expression Omnibus (GEO) under accession number GSE112049

DATA AVAILABILITY

RNA-seq data are deposited to the Gene Expression Omnibus (GEO) under accession number GSE112049.

All other data that support the findings of this study are available from the corresponding author upon request.

Abstract

Stem cells are maintained by transcriptional programs that promote self-renewal and repress differentiation. Here we found that the transcription factor c-Myb was essential for generating and maintaining stem cells within the CD8⁺ T cell memory compartment. Following viral infection, CD8⁺ T cells lacking *Myb* underwent terminal differentiation and generated fewer stem cell-like central memory cells than *Myb*-sufficient T cells. c-Myb acted both as a transcriptional activator of *Tcf7* (which encodes the transcription factor Tcf1) to enhance memory development and as a repressor of *Zeb2* (which encodes the transcription factor Zeb2) to hinder effector differentiation. Domain-mutagenesis experiments revealed that the transactivation domain of c-Myb was necessary for restraining differentiation, whereas its negative regulatory domain was critical for cell survival. *Myb* overexpression enhanced CD8⁺ T cell memory formation, polyfunctionality and recall responses that promoted curative antitumor immunity upon adoptive transfer. These findings identify c-Myb as a pivotal regulator of CD8⁺ T cell stemness and highlight its therapeutic potential.

Tissue homeostasis relies on the activity of a small population of adult stem cells that have the capacity to generate short-lived differentiated cells while maintaining their identity through self-renewal¹. Recently, in vivo clonogenic studies have revealed that within the mature T cell compartment, adult stem cells are confined to the CD62L⁺ memory T cell pool (which comprises stem cell-like memory (T_{SCM}) and central memory T (T_{CM}) cells)^{2, 3, 4}. There has been growing interest in the identification of the molecular, epigenetic and metabolic factors orchestrating the formation and maintenance of stem cell-like T cells, since these cells are known to be critical for the long-term efficacy of T cell-based immunotherapy and vaccines⁵.

It has become increasingly clear that several transcriptional networks regulating stem cell behavior are also utilized by T cells to promote the development and maintenance of stem cell-like memory cells and to restrain terminal effector differentiation^{5, 6}. For instance, Forkhead box protein O1 (Foxo1), T cell factor 1 (Tcf1), Signal transducer and activator of transcription 3 (STAT3) and the DNA-binding protein inhibitor Id3, which are essential for embryonic stem cell homeostasis and pluripotency^{7, 8, 9, 10}, have been shown to regulate T cell stemness and the formation of memory T cells^{11, 12, 13, 14, 15, 16}.

MYB—which encodes the transcription factor c-MYB—is highly expressed in human stem cell-like memory CD8⁺ T cells compared to both naïve and effector memory cells¹⁷. In mouse models, c-Myb regulates thymocyte development¹⁸ and regulatory T cell effector differentiation¹⁹, but its function in CD8⁺ T cells is unknown. Given the critical role of c-Myb in the regulation of stem cells and progenitor cells in diverse tissues, including the bone marrow, colonic crypts and neurogenic regions of the brain^{20, 21}, we hypothesized that it also plays a pivotal role in the regulation of stem cell-like behavior in T cells.

Herein, we determine that c-Myb is a critical regulator of CD8⁺ T cell stemness. c-Myb promoted pro-memory and survival programs via *Tcf7* (which encodes Tcf1) and *Bcl2* induction, and limited effector differentiation through *Zeb2* repression. We further show that while the c-Myb transactivation domain (TAD) is pivotal for restraining CD8⁺ T cell

differentiation, the negative regulatory domain (NRD) mediated cell survival processes. Finally, we demonstrate that the activity of c-Myb can be therapeutically harnessed to enhance the formation of stem cell-like T_{CM} cells and promote curative antitumor immunity in a melanoma model of adoptive immunotherapy.

RESULTS

c-Myb promotes the formation of stem cell-like T_{CM} cells by restraining terminal differentiation.

To evaluate the role of c-Myb in T cell differentiation we employed pmel-1 CD8⁺ T cells (which recognize the shared melanoma-melanocyte differentiation antigen gp100)²² carrying loxP-flanked *Myb* alleles. Because c-Myb plays critical roles during thymocyte development¹⁸, we bred a conditional knockout model based on a tamoxifen-regulated form of Cre (*Cre-ER^{T2}*)²³, pmel-1 *cre-ER^{T2} Myb^{fl/fl}*, to acutely delete *Myb* in mature CD8⁺ T cells (Fig. 1a). Naive pmel-1 *Myb^{-/-}* or pmel-1 *Myb^{+/+}* T cells isolated from littermates (Fig. 1b) were adoptively transferred into wild-type mice infected with a recombinant strain of vaccinia virus encoding gp100 (gp100-VV) and antigen-specific CD8⁺ T cell expansion and persistence was monitored over time (Fig. 1c). We found that in the absence of *Myb*, CD8⁺ T cells showed a minor defect in splenic accumulation during the acute phase of the immune response (Fig. 1d,e). However, following the peak of expansion, c-Myb-deficient T cell numbers contracted more sharply than wild-type cells, resulting in fewer memory cells one month after transfer. A steep decline in c-Myb deficient CD8⁺ T cell frequency during the contraction phase was similarly observed in lymph nodes (Supplementary Fig. 1a,b) and lungs (Supplementary Fig. 1c,d), underscoring the importance of c-Myb in cell maintenance.

To determine whether the reduced accumulation of c-Myb-deficient CD8⁺ T cells was due to defects in proliferation, we measured 5-bromo-2'-deoxyuridine (BrdU) uptake in transferred cells responding to gp100-VV infection. Early on, the vast majority of antigen-specific cells were vigorously proliferating, independent of the presence of c-Myb (Supplementary Fig. 2a,b). Surprisingly, a significant fraction of c-Myb-deficient T cells continued to uptake BrdU, while most wild-type CD8⁺ T cells stopped actively dividing at the peak of expansion (Supplementary Fig. 2a,b). Thus, reduced accumulation of *Myb^{-/-}* T cells was not caused by defective proliferation. Therefore, we determined if the differences in cell numbers were linked to a survival disadvantage. Measuring apoptosis with Annexin V revealed that in the absence of *Myb*, CD8⁺ T cells underwent massive apoptosis in the initial phase of the immune response (Supplementary Fig. 2c,d). This tendency, though not statistically significant, was also observed at the peak of the response (Supplementary Fig. 2c,d). These data emphasize a pivotal role of c-Myb in mature T cell survival, consistent with known findings in thymocytes^{18, 24}.

Increased turnover and apoptosis of pmel-1 *Myb^{-/-}* T cells might result from alteration of their differentiation program. We, therefore, evaluated the frequency of memory precursors and terminally differentiated effector (T_{TE}) cells by measuring the expression of KLRG1 and CD62L on transferred pmel-1 T cells five days after gp100-VV infection. The deletion of *Myb* resulted in a 4-fold increase of splenic KLRG1⁺CD62L⁻ T_{TE} cells and a dramatic loss of KLRG1⁻CD62L⁺ memory precursors compared to controls (Fig. 1f,g). Similarly,

there was a marked accumulation of T_{TE} cells and depletion of CD62L⁺ cells in c-Myb-deficient T cells in lymph nodes and lungs (Supplementary Fig. 3). These findings were also observed when physiological numbers of antigen-specific T cells²⁵ were transferred (data not shown). Although we did not measure major differences in perforin expression (data not shown), *Myb*-deficient T cells displayed higher amount of granzyme B (Fig. 1h) and enhanced killing capacity in vitro (Fig. 1i), further supporting the observation that c-Myb inhibits terminal effector differentiation. As T cells progressively differentiate into T_{TE} cells, they first lose the capacity to produce interleukin-2 (IL-2) and then tumor necrosis factor (TNF), before ultimately becoming monofunctional interferon (IFN)- γ producers²⁶. *Myb*^{-/-} T cells exhibited poor polyfunctionality as evidenced by the reduced frequency of IL-2⁺TNF⁺ + IFN- γ ⁺ cells (Fig. 1j,k). Notably, nearly half of cytokine producing *Myb*^{-/-} T cells were single IFN- γ producers, functionally consistent with our observation that CD8⁺ T cells were driven towards terminal differentiation in the absence of c-Myb. T cell differentiation is also intrinsically linked to changes in metabolism. For instance, effector T cells display reduced oxidative metabolism and mitochondrial spare respiratory capacity (SRC) compared to memory cells²⁷. Accordingly, *Myb*^{-/-} T cells displayed a lower basal oxygen consumption rate and a striking reduction in SRC compared to wild-type cells (Fig. 1l-n). Interestingly, these differences in cellular metabolism were in part independent of a skewed T_{TE} cell frequency as manifested by a small but significant reduction of mitochondrial fatty acid oxidation in *Myb*-deficient T cells after phenotypic normalization (Supplementary Fig.4). Taken together, phenotypic, functional and metabolic analyses concordantly demonstrate that c-Myb restrains CD8⁺ T cell terminal differentiation.

Consistent with a reduction of memory precursors generated in the acute phase of the immune response, we observed both decreased quantities of total memory cells (Fig. 1d,e) and frequencies of stem cell-like T_{CM} cells in *Myb*-deficient T cells 30 days after transfer (Fig. 1o,p). The hallmark function of memory cells is the ability to mount a robust response upon secondary infection. To determine whether *Myb*-deficient memory T cells were functionally competent, we transferred equal numbers of *Myb*^{-/-} or wild-type memory T cells into syngeneic hosts and measured their expansion 5 days after infection with a gp100 encoding adenovirus (gp100-Adv). Strikingly, we observed a dramatic impairment of *Myb*^{-/-} T cells to mount secondary immune responses (Fig. 1q,r). Altogether, these results demonstrate that c-Myb is essential for the generation of long-lived and functional stem cell-like T_{CM} cells.

c-Myb is indispensable for CD8⁺ T cell stemness

Persistence is a hallmark of stemness⁴. To determine the role of c-Myb in the persistence of CD8⁺ T cells we first evaluated the long-term maintenance of memory cells generated in the absence of *Myb* by measuring the frequency and number of adoptively transferred pmel-1 *Myb*^{-/-} or pmel-1 *Myb*^{+/+} T cells 90 days after infection with gp100-VV (Fig. 2a). Notably, we found a striking reduction of total and stem cell-like T_{CM} cell numbers in the spleens of mice that received *Myb*-deficient cells compared to controls (Fig. 2b,c). The reduction of *Myb*^{-/-} T cell numbers was not due to a skewed distribution because *Myb*^{-/-} T cells were similarly decreased in lungs and lymph nodes (Supplementary Fig. 5a-d). Compared to d30

(Fig. 1d,e), we observed wider differences in cell frequencies and numbers indicating that memory cells undergo progressive attrition in the absence of c-Myb.

Secondly, we determined the ability of *Myb*-deficient T cells to generate secondary memory cells. We transferred equal numbers of memory cells generated 45 days after primary infection into secondary recipients and assessed the frequency and number of pmel-1 *Myb*^{-/-} or pmel-1 *Myb*^{+/+} T cells one month after infection with gp100-Adv (Fig. 2d). *Myb*-deficient T cells exhibited a reduced capacity to form secondary memory cells in all organs evaluated (Fig. 2e,f and Supplementary Fig. 5e-h). More importantly, the generation of stem cell-like T_{CM} cells was markedly impaired as evidenced by a 98.8% reduction in splenic CD62L⁺ T cell numbers (Fig. 2g,h).

Finally, we tested the impact of *Myb*-deficiency on stem cell-like T_{CM} cell self-renewal. We labeled flow cytometric-sorted CD62L⁺ memory cells with carboxyfluorescein succinimidyl ester (CFSE) and transferred them into sub-lethally irradiated mice (Fig. 2i). Four weeks later, we measured CFSE dilution and maintenance of a stem cell-like phenotype under homeostatic proliferation. Wild-type cells displayed robust self-renewal as shown by the retention of CD62L expression on CFSE-diluted cells (Fig. 2j). *Myb*-deficient cells were unable to persist (Fig. 2j). Of note, only half of the few surviving cells were able to maintain their stem cell-like phenotype (Fig. 2j). Taken together, these experiments indicate that c-Myb is an essential regulator of CD8⁺ T cell stemness.

c-Myb enhances CD8⁺ T cell stemness by regulating *Tcf7*, *Bcl2* and *Zeb2* expression

To understand mechanisms by which c-Myb regulates CD8⁺ T cell differentiation, we performed RNA-seq of pmel-1 *Myb*^{+/+} and pmel-1 *Myb*^{-/-} CD8⁺ T cells harvested 5 days after adoptive transfer into mice infected with gp100-VV. To minimize skewing in gene expression due to differences in T cell subset distribution among *Myb*^{+/+} and *Myb*^{-/-} T cells, we analyzed KLRG1⁻CD62L⁻ cells sorted with a purity > 99% by flow cytometry (Supplementary Fig. 6a). Even after subset normalization, *Myb*^{-/-} T cells were enriched with genes known to be highly expressed in effector cells, whereas *Myb*^{+/+} T cells contained a higher proportion of transcripts associated with memory precursors (Fig. 3a, Supplementary Fig. 6b,c, and Supplementary Table 1). To elucidate downstream effectors of c-Myb, we filtered the dataset by selecting genes reported to be directly regulated (activated or repressed) by c-Myb in promyelocytes²⁸. *Bcl2*, a well-established target of c-Myb^{29, 30}, was downregulated in *Myb*^{-/-} T cells (Fig. 3a and Supplementary Table 1), in keeping with the survival defect observed in pmel-1 *Myb*^{-/-} T cells (Supplementary Fig 2c,d). Pathway analysis further revealed induction of transcriptional networks promoting cell death among *Myb*^{-/-} T cells (Supplementary Table 2). Two crucial transcription factors regulating CD8⁺ T cell differentiation, *Tcf7* and *Zeb2*^{13, 14, 31, 32} were differentially expressed in *Myb*^{-/-} and *Myb*^{+/+} cells (Fig. 3a and Supplementary Table 1). *Tcf7*, which enhances the formation and maintenance of memory T cells, was downregulated in *Myb*^{-/-} T cells. Conversely, *Zeb2*, a driver of CD8⁺ T cell terminal differentiation^{31, 32}, was upregulated in the absence of *Myb* (Fig. 3a). Gene Set Enrichment Analysis (GSEA) corroborated these findings by revealing that *Myb*^{-/-} T cells were enriched with genes upregulated in CD8⁺ T cells lacking WNT-

reporter activity³³ (Fig. 3b, left panel) and genes upregulated in *Zeb2*-sufficient CD8⁺ T cells³² (Fig. 3b, right panel).

To further elucidate the relationship of *Myb* expression with that of *Bcl2*, *Tcf7* and *Zeb2* during CD8⁺ T cell differentiation, we quantified the transcripts of these genes in naïve, CD62L⁺ and CD62L⁻ pmel-1 T cells generated in response to gp100-VV. As *Myb* expression declined with differentiation from naïve T cells into CD62L⁻ cells, *Bcl2* and *Tcf7* transcripts decreased (Fig. 3c,d), whereas *Zeb2* expression was inversely related to *Myb* expression (Fig. 3e). We next sought to evaluate how the genetic manipulation of *Myb* would affect *Bcl2*, *Tcf7* and *Zeb2* expression. To this end, we adoptively transferred into gp100-VV infected mice pmel-1 *Myb*^{+/+}, pmel-1 *Myb*^{-/-} and pmel-1 T cells transduced with *Myb*-Thy1.1 or Thy1.1 alone. Five days later, we analyzed *Bcl2*, *Tcf7* and *Zeb2* expression in transferred T cells. Reinforcing our RNA-seq results, *Myb* deletion resulted in significant reduction of *Bcl2* and *Tcf7* (Fig. 3f,g), while dramatically increasing *Zeb2* expression (Fig. 3h). By contrast, *Myb* overexpression enhanced both *Bcl2* and *Tcf7* (Fig. 3f,g) and suppressed *Zeb2* expression (Fig. 3h). Similar findings were obtained by measuring *Bcl2* and *Tcf1* proteins (Fig. 3i,j). The lack of working mouse *Zeb2*-specific antibodies prevented assessment of the impact of c-Myb on *Zeb2* protein expression. Transcriptional regulation of *Tcf7* by c-Myb was confirmed by a *Tcf7GFP* reporter assay in CD8⁺ T cells after overexpression of *Myb* (data not shown). *Bcl2* is regulated by c-Myb³⁰. Whether c-Myb directly binds and regulates *Tcf7* and *Zeb2* expression in CD8⁺ T cells merited further analysis. We performed chromatin immunoprecipitation (ChIP) followed by quantitative PCR in pmel-1 *Myb*^{+/+} and *Myb*^{-/-} CD8⁺ T cells and found a specific enrichment of *Tcf7* enhancer and *Zeb2* promoter regions with c-Myb immunoprecipitation in wild-type cells but not in *Myb*^{-/-} T cells (Fig. 3k). Taken together, these findings place c-Myb as a transcriptional activator of *Bcl2* and *Tcf7*, and as a transcriptional repressor of *Zeb2* in CD8⁺ T cells.

We next sought to determine if the tendency for *Myb*^{-/-} T cells to undergo terminal differentiation depends on insufficient levels of *Tcf7* and unrestrained expression of *Zeb2*. To this end, we adoptively transferred pmel-1 *Myb*^{-/-} T cells and pmel-1 *Myb*^{-/-} *Zeb2*^{+/+} T cells transduced with either *Tcf7-GFP* or *GFP* alone in gp100-VV infected mice and evaluated the formation of KLRG1⁺CD62L⁻ T_{TE} cells in comparison with pmel-1 *Myb*^{fl/fl} transduced with *GFP* control. Testing complete *Zeb2* deficiency on pmel-1 *Myb*^{-/-} T cells was not possible. The *Zeb2* loci is located on chromosome 2, just 12 centimorgans from the insertion site of the pmel-1 *Tcra* and *Tcrb* transgenes²², therefore there is a slim probability of obtaining a *Zeb2*^{fl/fl} with pmel-1 background. Consistent with our results using naïve CD8⁺ T cells (Fig. 1f,g), *in vitro* activated pmel-1 cells engineered to express *GFP* alone generated higher frequencies of T_{TE} cells in the absence of *Myb* (Fig. 3l,m top). Individually, overexpression of *Tcf7* or *Zeb2* haploinsufficiency significantly reduced the frequency of T_{TE} cells in pmel-1 *Myb*^{-/-} *GFP*T cells, though *Zeb2* depletion had a more pronounced effect (Fig. 3l,m top). Remarkably, the combination of both genetic approaches completely rescued the skewed differentiation pattern of pmel-1 *Myb*^{-/-} *GFP*T cells (Fig. 3l,m top). Despite correcting the differentiation program, these genetic maneuvers did not rescue the survival defects of pmel-1 *Myb*^{-/-} T cells, implicating *Bcl2* and other downstream factors behind the pro-survival function of c-Myb (Fig. 3l,m bottom). Thus, c-

Myb promotes CD8⁺ T cell stemness both by inducing pro-memory and survival programs via *Tcf7* and *Bcl2*, and by restraining effector differentiation through suppression of *Zeb2*.

Distinct functions of c-Myb domains in the regulation of CD8⁺ T cell differentiation and survival

To further characterize the molecular mechanisms by which c-Myb regulates CD8⁺ T cell differentiation and survival, we generated a complement of *Myb* mutants and tested their ability to rescue the phenotype of pmel-1 *Myb*^{-/-} T cells. We compared full length *Myb* activity to that of three different *Myb* mutants³⁴: a truncated *Myb* lacking the NRD (*Myb* 1–330); a *Myb* mutant with a non-functional TAD (glycine, proline insertion after the 304-amino acid residue, *Myb* 304GP); and a truncated *Myb* comprising the DNA binding domain only (*pBind*) (Fig. 4a). These *Myb* mutants were cloned into a MSGV-Thy1.1 retroviral vector to allow sorting and tracking of transduced pmel-1 cells after adoptive transfer into wild-type mice infected with gp100-VV (Fig. 4a). With the exception of the *pBind* construct, which resulted in higher levels of *Myb* transcription, all other vectors induced comparable levels of *Myb* transcripts (data not shown). As we previously observed, pmel-1 *Myb*^{-/-} Thy1.1 CD8⁺ T cells generated higher frequencies of T_{TE} cells at the peak of the immune response compared to pmel-1 *Myb*^{+/+} Thy1.1 T cells (Fig. 4b,c). As expected, full length *Myb* significantly reduced the percentage of T_{TE} cells (Fig. 4b,c). Strikingly, *Myb* (1–330) not only abrogated the generation of T_{TE} cells but also dramatically increased the frequency of CD62L⁺ memory precursors (Fig. 4b,c), confirming NRD self-regulation of *Myb* in CD8⁺ T cells. Conversely, *Myb* *pBind* and 304GP failed to rescue the phenotype of pmel-1 *Myb*^{-/-} T cells (Fig. 4b,c) demonstrating the indispensable function of the c-Myb TAD in restraining CD8⁺ T cell terminal differentiation. Notably, these functional differences among *Myb* mutants correlated with their abilities to induce *Tcf7* expression and repress *Zeb2* transcription. Full length *Myb* and *Myb* (1–330), which both inhibited CD8⁺ T cell terminal differentiation, promoted *Tcf7* expression and decreased *Zeb2* transcripts compared to pmel-1 *Myb*^{-/-} Thy1.1 CD8⁺ T cells (Fig. 4d,e). On the other hand, *Myb* *pBind*, which did not rescue the phenotype of pmel-1 *Myb*^{-/-} T cells, did not lower *Zeb2* expression and failed to induce *Tcf7* (Fig. 4d,e). Interestingly, *Myb* 304GP, which was inefficient in inhibiting CD8⁺ T cell differentiation, did retain high levels of *Zeb2* and induce *Tcf7*, albeit to a lesser extent than full length *Myb* (Fig. 4d,e). This emphasizes the prominent role of *Zeb2* over *Tcf7* in the regulation of T_{TE} cells. Thus, the c-Myb TAD restrains CD8⁺ T cell differentiation by promoting *Tcf7* expression but mostly by suppressing *Zeb2* transcription. Despite being unable to correct CD8⁺ T cell differentiation, *Myb* 304GP fully rescued the frequency and total number of pmel-1 *Myb*^{-/-} CD8⁺ T cells (Fig. 4f,g). Evidently, the pro-survival effects of c-Myb are independent of its TAD activity and its regulation of *Tcf7* and *Zeb2* (Fig. 3l,m, bottom). Further substantiating this conclusion, is the finding that *Myb* (1–330), which markedly inhibited CD8⁺ T cell differentiation, induced *Tcf7* and suppressed *Zeb2* expression, but did not increase pmel-1 T cell frequency and total number to the levels produced in *Myb*^{+/+} T cells (Fig. 4f,g). Combined with the results from *Myb* *pBind* complementation (Fig. 4f,g), the pro-survival activity of c-Myb is primarily linked to the integrity of its C-terminal domain. In summary, the c-Myb TAD is critical for regulating CD8⁺ T cell differentiation, but it is the NRD that is essential for maintaining cell survival.

Enforced *Myb* expression enhances CD8⁺ T cell stemness and polyfunctionality

Having demonstrated the pivotal role of c-Myb in the regulation of CD8⁺ T cell stemness, we next sought to determine if the generation of stem cell-like T_{CM} cells could be enhanced by enforcing *Myb* expression. We transduced pmel-1 Ly5.1⁺ CD8⁺ T cells with *Myb*-Thy1.1 and pmel-1 Ly5.2⁺ CD8⁺ T cells with Thy1.1 alone, mixed them at 1:1 ratio, and co-transferred into wild-type mice infected with gp100-VV (Fig. 5a). Overexpression of c-Myb enhanced the expansion of splenic antigen-specific pmel-1 T cells, which accumulated at 4-fold the rate of controls at the peak of the immune response (Fig 5b,c). Likewise, we observed an increased expansion of *Myb*-overexpressing pmel-1 T cells in lungs and lymph nodes, though the accumulation was more pronounced in the latter (Supplementary Fig. 7a–d). Enforcing *Myb* expression did not increase the numbers of pmel-1 T cells in the spleen and lungs thirty days after transfer (Fig 5b,c and Supplementary Fig. 7a,b), indicating that c-Myb overexpression alone is insufficient to cause unrestrained T cell expansion or transformation²⁰. We observed, however, a dramatic increase of pmel-1 T cells (~50-fold) in the lymph nodes (Supplementary Fig. 7c,d), which prompted us to investigate whether the increased accumulation of *Myb*-overexpressing T cells in the lymph nodes was due to the preferential formation of stem cell-like T_{CM} cells, which preferentially home to lymphoid tissues. Consistent with our findings using c-Myb-deficient T cells, we found that overexpression of c-Myb promoted the generation of stem cell-like T_{CM} cells while restraining terminal effector differentiation (Fig. 5d,e and Supplementary Fig. 7e,f). These results were further strengthened by functional studies, which revealed that *Myb*-overexpressing cells displayed enhanced polyfunctionality and a sustained capacity to produce IL-2 (Fig. 5f–h). Taken together these results demonstrate that increasing *Myb* levels in CD8⁺ T cells is an effective strategy to generate polyfunctional stem cell-like T_{CM} cells.

Enforced expression of *Myb* enhances CD8⁺ T cell recall responses and antitumor immunity

The hallmark of memory cells is their capacity to rapidly proliferate and differentiate into a massive number of effectors upon secondary infection. To determine if the enhanced generation of stem cell-like T_{CM} cells resulting from c-Myb overexpression would promote stronger recall responses, we re-challenged mice that were initially infected with gp100-VV with gp100-adV (Fig. 6a). Strikingly, the accumulation of splenic *Myb*-overexpressing T cells at the peak of the secondary immune response was 10-fold higher in frequency and number as compared to controls (Figure 6b,c). Repeated antigen-stimulations are known to drive CD8⁺ T cells towards terminal differentiation^{35, 36}. To determine whether terminal differentiation could be restrained by overexpressing c-Myb, we measured T_{TE} cells after secondary infection with gp100-adV. Remarkably, c-Myb overexpression not only dramatically reduced the frequencies of T_{TE} cells in both peripheral and lymphoid tissues (Fig. 6d–i), but also maintained a higher fraction of stem cell-like T_{CM} cells. Moreover, intracellular cytokine staining analyses showed a marked reduction of terminally differentiated, monofunctional IFN- γ producers in the *Myb*-overexpression group (Fig. 6j–l).

It is well-established that the dose of adoptively transferred tumor-specific CD8⁺ T cells correlates with the magnitude of tumor regression³⁷. Generating large numbers of tumor-reactive T cells in vitro, however, can be counterproductive because as cells expand they progressively differentiate into T_{TE} cells with limited therapeutic fitness³⁵. We sought to determine whether overexpression of c-Myb would not only generate larger cell numbers through repetitive antigenic stimulations but also preserve a larger number of stem cell-like T_{CM} cells. As we previously showed, antigen re-stimulation induced the formation of CD62L⁻ effector cells (Fig. 7a,b). By contrast, the vast majority of pmel-1 T cells overexpressing c-Myb retained high CD62L expression throughout multiple stimulations (Fig. 7a,b). Notably, restimulated T cells preserved their mitochondrial mass only when c-Myb was constitutively overexpressed (Fig. 7c,d). Even after a multi-log expansion *Myb*-overexpressing T cells exhibited significant SRC and fatty acid metabolism (Fig. 7 e-g), highlighting the importance of c-Myb in the maintenance of metabolic fitness. To evaluate their therapeutic efficacy, we adoptively transferred multiply stimulated, *Myb*-overexpressing pmel-1 T cells into mice bearing subcutaneous B16-hgp100 melanomas in conjunction with administration of IL-2. *Myb*-overexpressing T cells triggered curative responses in all mice, whereas controls cells failed to cure 4/5 animals (Fig. 7h). Conversely, the antitumor efficacy of pmel-1 T cells was severely impaired in the absence of c-Myb (data not shown). To determine if the transfer of stem cell-like T_{CM} cells in the *Myb*-overexpression group conferred long-lasting antitumor memory responses we re-challenged the surviving animals with tumors around 200 days after the primary T cell transfer. Remarkably, tumors did not grow in any of the re-challenged animals (Fig. 7h), indicating that overexpression of c-Myb enhances the establishment of long-lived immunological memory. Consistent with this observation, we found increased numbers of memory T cells in the surviving mice that received *Myb*-overexpressing T cells 470 days earlier (Supplementary Fig. 8a,b). Although all memory T cells displayed a stem cell-like T_{CM} phenotype (Supplementary Fig.8c), a larger fraction of *Myb*-overexpressing T cells was capable of producing IL-2 compared to controls (Supplementary Fig.8d). Taken together, these findings highlight the therapeutic potential of maneuvers aimed at increasing c-Myb activity in CD8⁺ T cells.

DISCUSSION

The molecular programs regulating the formation and maintenance of stem cell-like T_{CM} cells remains unresolved. In this current study, we identified c-Myb as a master regulator of CD8⁺ T cell stemness. In the absence of c-Myb, antigen-stimulated CD8⁺ T cells are driven toward terminal effector differentiation and are prone to apoptosis resulting in both quantitative and qualitative impairment of memory responses. These conclusions are further supported by the observation that CD8⁺ T cells deficient in the microRNA miR-150, a known inhibitor of c-Myb, have enhanced propensity to form long-lived memory T cells³⁸. Our findings run in parallel to those in stem cells and progenitor cells where c-Myb is seen to restrain differentiation^{20, 21}, illuminating a conserved molecular program regulating self-renewal and differentiation⁵.

Mechanistically, we demonstrated that c-Myb enhances CD8⁺ T cell survival and memory development by promoting the expression of the anti-apoptotic molecule *Bcl2* and by

inducing *Tcf7*, a transcription factor essential to the formation and maintenance of stem cell-like T_{CM} cells^{13, 14}. Recently, *Tcf1* expression has also been associated with the maintenance of CXCR5⁺Tim3⁻ stem cell-like T cells in chronic infection and cancer^{39, 40, 41, 42}. Future work will determine whether c-Myb plays an important role in maintaining this cell population. We further demonstrated that c-Myb also actively repressed pro-differentiating programs by inhibiting the transcription of *Zeb2*, which we have recently identified as a major driver of terminal effector differentiation³¹. This result further emphasizes the understudied repressive function of c-Myb, often considered a transcriptional activator. The repressive activity of c-Myb has been linked to its competitive binding with positive transcription regulators to target gene promoters⁴³ and to the recruitment of cell type-specific repressors^{44, 45}. While we haven't formally addressed the latter mechanism, complementation studies with the *pBind* mutant unequivocally exclude a mechanism of competition with positive transcription regulators as the c-Myb DNA-binding domain failed to suppress *Zeb2* transcription and restore physiologic numbers of memory precursors on its own. Recently, it has been proposed that c-Myb-mediated repression might paradoxically involve its interaction with the coactivator p300 possibly through the induction of repressive non-coding RNAs²⁸. Consistent with this view, we found that *Myb 304GP* which has been shown to have an impaired ability to recruit p300³⁴ was unable to repress *Zeb2* and inhibit terminal effector differentiation.

Our complementation studies also indicate that the C-terminal NRD domain of c-Myb has an important function in regulating CD8⁺ T cell survival. The mechanistic basis of this finding remains to be elucidated. Myb NRD contains an EVES motif which has been shown to bind p100⁴⁶. Although p100 overexpression inhibited the transcriptional activity of c-Myb in in vitro cultured fibroblasts⁴⁶, this molecule has been demonstrated to function as a coactivator in other settings⁴⁷ possibly implicating its involvement in the pro-survival programs triggered by c-Myb.

Finally, our study has profound therapeutic implications for T cell-based immunotherapy. Uncoupling T cell differentiation from T cell expansion has been sought after as the Holy Grail of adoptive immunotherapy as the therapeutic efficacy highly depends on both the cell dose and differentiation status of infused T cells^{37, 48}. Thus far strategies that have been shown to effectively promote stem cell-like memory T cells have the downside effect of impairing cell expansion^{4, 17, 49, 50}. Overexpression of c-Myb not only preserved CD8⁺ T cell stemness by inhibiting differentiation, but also allowed a better cell yield, resulting in curative antitumor responses and the establishment of long-term immunologic memory. The *Myb* platform may ultimately pave new avenues for the generation of cell-based immunotherapy based on the adoptive transfer of stem cell-like T_{CM} cells.

ONLINE METHODS

Mice

C57BL/6NCr and B6-Ly5.1/Cr were from Charles River Frederick Research Model Facility; pmel-1 (B6. Cg-*Thy1^l/Cy Tg(TcraTcrb)8Rest/J*) mice were from the Jackson Laboratory; Cre-ER^{T2} (B6-*Gt(ROSA)26Sor^{tm9(cre/Esr1)Arctc}*) mice were from Taconic. *Myb^{fl/fl}* mice¹⁸ were obtained from Timothy Bender, University of Virginia, Charlottesville, VA and were

back-crossed with C57BL/6NCr mice for >30 generations, USA; *Zeb2^{fl/fl}* mice were kindly obtained from Susan Kaech, Yale University, New Haven, CT, USA. Pmel-1 mice were crossed with *Myb^{fl/fl}* mice for the generation of pmel-1 *Myb^{fl/fl}* mice and were further crossed with *Cre-ERT2* mice for the generation of pmel-1 *Cre-ERT2 Myb^{fl/fl}* mice. pmel-1 *Cre-ERT2 Myb^{fl/fl}* mice were further crossed with *Zeb2^{fl/fl}* mice to obtain pmel-1 *Cre-ERT2 Myb^{fl/fl} Zeb2^{w^t/fl}* mice. Splens from *Tcf7^{GFP/+}* mice⁵¹ were obtained from Avinash Bhandoola, National Cancer Institute and Hai-Hui Xue, Iowa University. All mouse experiments were done with the approval of the National Cancer Institute Animal Care and Use Committee.

Cell lines

Platinum-E cells were obtained from Cell Biolabs following authentication and validation as being mycoplasma free. B16 melanoma expressing human gp100 (B16-hgp100)⁵² were provided by Ken-ichi Hanada, National Cancer Institute, Bethesda, MD and validated as being mycoplasma free via a PCR-based assay.

Antibodies, flow cytometry and cell sorting

Anti-BrdU (3D4), anti-Ly5.2 (104), anti-Thy1.1 (OX-7), anti-CD62L (MEL-14), anti-IFN γ (XMG1.2), anti-TNF (MP6-XT2) were from BD Biosciences; anti-CD8 α (53–6.7), anti-KLRG-1 (2F1), anti-IL-2 (JE56–5H4), anti-CD44 (IM7), Bcl-2 (633504), anti-mouse Perforin Antibody (S16009A), anti-human/mouse granzyme B Antibody (GB11) were from Biolegend; anti-TCF1 (C63D9) was from Cell Signaling Technology. For intracellular staining of Tcf1, Bcl-2, granzyme B and perforin, cells were fixed and permeabilized (eBioscience, 00–5524). Leukocyte Activation Cocktail containing phorbol myristate acetate (PMA) and ionomycin (BD Biosciences) was used to stimulate T cells for intracellular cytokine staining. A Fixation/Permeabilization Solution Kit (BD Biosciences) was used to fix and permeabilize the cells. Annexin V staining was performed with Annexin V Apoptosis Detection Kit (eBiosciences). BrdU staining was performed with BrdU Staining Kit (eBiosciences) following the protocol provided by the manufacturer. LSR II or BDFortessa (BD Biosciences) were used for flow cytometry acquisition. Samples were analyzed with FlowJo software (TreeStar). Naive CD8⁺ T cells were enriched using Naïve CD8⁺ T cell isolation kit from Stem Cell Technology. A FACS Aria (BD Biosciences) was employed for all other T cell enrichments.

Real-time RT-PCR

RNA was isolated with an RNeasy Mini Kit (Qiagen). Reverse transcription PCR was performed to obtain cDNA (Applied Biosystems). Primers from Applied Biosystems and a Prism 7900HT (Applied Biosystems) were used for real-time PCR using Fast Start Universal SYBER GREEN Master (Roche). Results are presented relative to *Actb* or *Rpl13* expression.

List of primers used:

Rpl13 β : CGAGGCATGCTGCCCCACAA

Rpl13R: AGCAGGGACCACCATCCGCT

Bcl2F: GTCGCTACCGTCGTGACTTC

Bcl2R: CAGACATGCACCTACCCAGC

Zeb2F: CCACGCAGTGAGCATCGAA

Zeb2R: CAGGTGGCAGGTCATTTTCTT

MybF: AGACCCCGACACAGCATCTA

MybR: CAGCAGCCCATCGTAGTCAT

Tcf7F: AGCTTTCTCCACTCTACGAACA

Tcf7R: AATCCAGAGAGATCGGGGGTTC

EomesF: GCGCATGTTTCCTTTCTTGAG

EomesR: GGTCGGCCAGAACCACTTC

Tbx21F: AGCAAGGACGGCGAATGTT

Tbx21R: GGGTGGACATATAAGCGGTTC

Prdm1F: TTCTCTTGGA AAAACGTGTGGG

Prdm1R: GGAGCCGGAGCTAGACTTG

Bach2F: TCAATGACCAACGGAAGAAGG

Bach2R: GTGCTTGCCAGAAGTATTTCACT

Immunoblot analysis

Proteins were separated by 4–12% SDS-PAGE, followed by standard immunoblot analysis with anti-Myb (Millipore, clone 1–1), anti-GAPDH (6C5; Santa Cruz Biotechnology), horseradish peroxidase–conjugated goat anti–mouse IgG (sc-2031; Santa Cruz Biotechnology) and horseradish peroxidase–conjugated goat anti–rabbit IgG (sc-2030; Santa Cruz Biotechnology).

Chromatin Immunoprecipitation

5 day *in vitro* cultured cells were crosslinked to chromatin by adding 1% formaldehyde to each culture dish at room temperature for 10 minutes and stopped by addition of 125 mM glycine followed by incubation at room temperature for 5 minutes. Cells were harvested, pelleted and washed with cold PBS. Cells were resuspended at 10^7 cells/ml in cold cytoplasmic lysis buffer (20 mM Tris-HCl pH 8, 85 mM KCl, 0.5% NP-40, 1 mM PMSF and EDTA-free protease inhibitor mixture (Roche)) and incubated on ice for 10 minutes. Nuclei were centrifuged, resuspended at 10^7 cells/ml in cold sonication buffer (10mM Tris-

HCl pH 8, 0.1 mM EDTA, 1% NP-40, 0.01% SDS, 1 mM PMSF and EDTA-free protease inhibitor mixture) and sonicated using a Branson 450 sonifier to generate chromatin fragment. Debris was cleared by centrifugation and chromatin was supplemented with 5% glycerol and 127 mM NaCl. Chromatin aliquots of 500 μ l were pre-cleared using protein A agarose slurry (Millipore, Bedford, MA) for 1 hour and immunoprecipitated over night with anti-Myb (A304–138A; Bethyl) or mouse IgG2a, κ isotype control (BD Biosciences, San Jose, CA) with rotation at 4°C. Immune complexes were collected with protein A agarose slurry for 1 hour with rotation at 4°C. Beads were washed for 5 minutes with rotation at 4°C with low salt buffer (10 mM Tris-HCl pH8, 2 mM EDTA, 0.1% SDS, 1% NP40, 150 mM NaCl), high salt buffer (10 mM Tris-HCl pH8, 2 mM EDTA, 0.1% SDS, 1% NP40, 500 mM NaCl), LiCl buffer (10 mM Tris-HCl pH8, 1mM EDTA, 1% Deoxycholate, 1% NP40, 250 mM LiCl) and twice in TE. All wash buffers were supplemented with protease inhibitors and PMSF. Bound complexes were eluted off the beads in 500 μ l elution (0.1 M, 1% SDS) buffer with rotation at room temperature for 30 minutes. Formaldehyde crosslinking was reversed in the presence of 200 mM NaCl at 65°C overnight. DNA was phenol/chloroform extracted following RNase A and proteinase K treatment.

ChIP PCR primers

Tcf7 5' - ATAACTGGTGCCATGACCGG-3'

Tcf7R 5' - CAGGGCTGGACAACACAAAG -3'

Zeb2 primers were from Qiagen (GPM1048638(+04A).

Retroviral vector construction and virus production

Myb isoform 2 or its mutants' cDNA was cloned together into the MSGV-1-Thy1.1 vector as previously described¹⁶. Platinum-E cell lines were used for gamma-retroviral production by transfection with DNA plasmids through the use of Lipofectamine 2000 (Invitrogen) and collection of virus 40 h after transfection. pMIG empty vector and *Tcf7*-pMIG were obtained from Avanish Bhandoola, National Cancer Institute, Bethesda, MD, USA.

In vitro activation and transduction of CD8⁺ T cells

Naïve CD8⁺ T cells were activated on plates coated with anti-CD3 ϵ (2 μ g/ml; 145–2C11; BD Biosciences) and soluble anti-CD28 (1 μ g/ml; 37.51; BD Biosciences) in culture medium containing recombinant human IL-2 (10 ng/ml; Prometheus Laboratories Inc). Virus was 'spin-inoculated' at 2,000g for 2 h at 32 °C onto plates coated with retronectin (Takara). CD8⁺ T cells activated for 24 h were spun onto plates after aspiration of viral supernatants. Transduction efficiency was then evaluated 48h later.

Tamoxifen treatment, adoptive cell transfer, infection, and tumor challenge

Cre-ERT2-mediated deletion of floxed alleles was induced by intraperitoneal injection of 2 mg tamoxifen (Sigma-Aldrich) dissolved in corn oil (Sigma-Aldrich) for 4 consecutive days. Pmel-1 CD8⁺ T cells (600–3 X 10⁵ cells) were adoptively transferred into 6–10-week old C57BL/6 followed by infection with 2 X 10⁷ PFU recombinant vaccinia virus expressing human gp100 (gp100-VV). Recall response experiments were performed 30–45 days after

primary infection with gp100-VV by either re-challenging mice with 10^8 PFU recombinant adenovirus type 2 expressing human gp100 or by performing secondary adoptive transfer of normalized memory cell numbers. For homeostatic proliferation of memory CD8⁺ T cells, recipient mice were sub-lethally irradiated (5Gy) prior to cell transfer. For tumor experiments 6–10-week old C57BL/6 mice were injected subcutaneously with 2×10^5 B16-hgp100. Mice were treated 10 days later with intravenous injection of 5×10^6 pmel-1 CD8⁺ T cells. Mice were vaccinated intravenously with 2×10^7 pfu gp100-VV and recombinant human IL-2 (2.4e5 IU/dose) was administered twice a day for a total of 6 doses. For long-term memory and secondary transfer experiments we employed recipient mice carrying the *Myb*^{fl} allele to avoid possible rejection. In these experiments, we used pmel CD8⁺ T cells from tamoxifen-treated littermates carrying the *Myb*^{fl} allele but not cre^{ERT2} as WT controls.

Quantification of adoptively transferred cells

Spleens were processed and cells were counted by trypan blue exclusion of dead cells. The frequency of transferred T cells was determined by measurement of the expression of CD8 and Thy1.1 or GFP or Thy1.1/Ly5.1 or Ly5.2 by flow cytometry. The absolute number of pmel-1 cells was calculated by multiplying the total cell count by the percentage of CD8⁺GFP⁺, CD8⁺Thy1.1⁺ or CD8⁺Thy1.1⁺ Ly5.1⁺ cells or CD8⁺Ly5.2⁺.

Bioenergetic analyses

CD8⁺ T cells were re-suspended in serum-free unbuffered DMEM medium (Sigma-Aldrich) supplemented with L-glutamine (200 mM), NaCl (143 mM), D-glucose (25 mM), and sodium pyruvate (1 mM). Cells were then plated onto Seahorse cell plates (10^6 cells per well), coated with Cell-Tak (Corning) to facilitate T cell attachment. Mitochondrial stress test was performed by measuring OCR (pmol/min) at steady state and after sequential injection of oligomycin (0.5 μ M), FCCP (0.5 μ M), rotenone (1 μ M) and antimycin A (1 μ M) (Sigma-Aldrich). In some experiments, etomoxir (43 μ M) was injected prior to rotenone and antimycin A. Experiments with the Seahorse system utilized the following assay conditions: 2 min mixture; 2 min wait; and 3 min measurement.

RNA-seq

RNA concentration was determined with the Qubit RNA broad range assay in the Qubit Fluorometer (Invitrogen) and RNA integrity was determined with Eukaryote Total RNA Nano Series II Chip on a 2100 Bioanalyzer (Agilent). RNA-seq libraries were prepared from 4 μ g of total RNA via the TruSeq RNA sample prep kit according to manufacturer's protocol (Illumina). In brief, oligo-dT purified mRNA was fragmented and subjected to first and second strand cDNA synthesis. cDNA fragments were blunt-ended, ligated to Illumina adaptors, and PCR amplified to enrich for the fragments ligated to adaptors. The resulting cDNA libraries were verified and quantified on Agilent Bioanalyzer and sequencing (2 \times 75 bp paired-end) was conducted on GAIIX Genome Analyzer (Illumina). RNA-seq analyses were performed using 3 biological replicates. RNA sequencing was performed and analyzed as described previously. Briefly, total RNA was prepared from cells using the RNeasy Plus Mini Kit (Qiagen). 200 ng total RNA was subsequently used to prepare RNA-seq library by using TruSeq RNA sample prep kit (FC-122–1001, Illumina) according to the manufacturer's instructions. Sequenced reads were aligned to the mouse genome (NCBI37/

mm9) with TopHat 2.0.11⁵³, and uniquely mapped reads were used to calculate gene expression. The mouse genome reference sequences (mm9) and the genome annotation were downloaded from the UCSC genome browser for RNA-seq analysis. Raw counts that fell on transcripts of each gene were calculated, and differentially expressed genes were identified with the statistical R package DESeq2⁵⁴. Differentially expressed genes were required to meet to the criteria: fold change > 1.5 or < 1.5, and false discovery rate < 0.05. Expression heatmaps were generated with the Bioconductor Package ComplexHeatmap⁵⁵.

Gene-Set enrichment and pathway analyses

Mouse gene symbols were first mapped to the orthologous human genes using the homology information available from the MGI website (ftp://ftp.informatics.jax.org/pub/reports/HMD_HGNC_Accession.rpt) and were ranked by the fold changes of the gene expression as profiled by RNA-seq. Then, gene set enrichment was analyzed using GSEA software (<http://software.broadinstitute.org/gsea/downloads.jsp>)⁵⁶. Pathway Analysis was performed on the identified differentially expressed genes list using the Core Analysis function included in Ingenuity Pathway Analysis (IPA, Qiagen).

CFSE and MitoTracker Green labeling

CD8⁺ T cells were incubated with 1 μ L of CFSE (Thermo Fischer # C34554) in 1ml protein-free PBS for 20 minutes at 37°C with agitation followed. For MitoTracker Green staining, CD8⁺ T cells were incubated with 250nM MitoTracker Green FM (Molecular Probes) for 30 minutes at 37°C.

Cytolytic assay

Target cell lysis was evaluated with the xCELLigence Real-Time Cell Analyzer (ACEA Biosciences). Electrical impedance due to B16-hgp100 was measured every 15 minutes until the end of the experiment. The data were processed using the xCELLigence RTCA software package (version 2.0), and the results are reported as a cell index value (CI), where $CI = (\text{impedance at time point } n - \text{impedance in the absence of cells}) / \text{nominal impedance value}$. CI was normalized to 1 at the time when T cells were added. Percentage of lysis was calculated for values obtained after 18h of co-culture and different T cell:B16-hgp100 ratios.

Statistical analyses

Using Graphpad Prism 7, a two-tailed Student's t-test was used for comparison of data such as gene expression levels, cell proliferation and functionality (numbers and percentage), and tumor growth slopes. A Log-rank (Mantel-Cox) Test was used for comparison of survival curves.

Reporting summary.

Further information on research design is available in the Nature Research Reporting Summary linked to this article.

Supplementary Material

Refer to Web version on PubMed Central for supplementary material.

ACKNOWLEDGMENTS

This work was supported by the Intramural Research Program of the US National Institutes of Health, National Cancer Institute, Center for Cancer Research (ZIABC011480) (to L.G.); the US National Institutes of Health grants (GM100776 and CA85842) (to T.P.B); the Wellcome Trust/Royal Society (105663/Z/14/Z), the UK Biotechnology and Biological Sciences Research Council (BB/N007794/1), and Cancer Research UK (C52623/A22597) (to R.R). We thank K. Hanada for providing B16 (H-2^D)-hgp100. This work used the computational resources of the NIH HPC Biowulf cluster (<http://hpc.nih.gov>).

REFERENCES

1. Simons BD & Clevers H Strategies for homeostatic stem cell self-renewal in adult tissues. *Cell* 145, 851–862 (2011). [PubMed: 21663791]
2. Graef P et al. Serial transfer of single-cell-derived immunocompetence reveals stemness of CD8(+) central memory T cells. *Immunity* 41, 116–126 (2014). [PubMed: 25035956]
3. Gattinoni L Memory T cells officially join the stem cell club. *Immunity* 41, 7–9 (2014). [PubMed: 25035947]
4. Gattinoni L, Speiser DE, Lichterfeld M & Bonini C T memory stem cells in health and disease. *Nature medicine* 23, 18–27 (2017).
5. Gattinoni L, Klebanoff CA & Restifo NP Paths to stemness: building the ultimate antitumour T cell. *Nature reviews. Cancer* 12, 671–684 (2012). [PubMed: 22996603]
6. Thaventhiran JE, Fearon DT & Gattinoni L Transcriptional regulation of effector and memory CD8+ T cell fates. *Current opinion in immunology* 25, 321–328 (2013). [PubMed: 23747000]
7. Zhang X et al. FOXO1 is an essential regulator of pluripotency in human embryonic stem cells. *Nat Cell Biol* 13, 1092–1099 (2011). [PubMed: 21804543]
8. Yi F et al. Opposing effects of Tcf3 and Tcf1 control Wnt stimulation of embryonic stem cell self-renewal. *Nat Cell Biol* 13, 762–770 (2011). [PubMed: 21685894]
9. Niwa H, Burdon T, Chambers I & Smith A Self-renewal of pluripotent embryonic stem cells is mediated via activation of STAT3. *Genes & development* 12, 2048–2060 (1998). [PubMed: 9649508]
10. Ying QL, Nichols J, Chambers I & Smith A BMP induction of Id proteins suppresses differentiation and sustains embryonic stem cell self-renewal in collaboration with STAT3. *Cell* 115, 281–292 (2003). [PubMed: 14636556]
11. Hess Michelini R, Doedens AL, Goldrath AW & Hedrick SM Differentiation of CD8 memory T cells depends on Foxo1. *The Journal of experimental medicine* 210, 1189–1200 (2013). [PubMed: 23712431]
12. Kim MV, Ouyang W, Liao W, Zhang MQ & Li MO The transcription factor Foxo1 controls central-memory CD8+ T cell responses to infection. *Immunity* 39, 286–297 (2013). [PubMed: 23932570]
13. Jeannot G et al. Essential role of the Wnt pathway effector Tcf-1 for the establishment of functional CD8 T cell memory. *Proceedings of the National Academy of Sciences of the United States of America* 107, 9777–9782 (2010). [PubMed: 20457902]
14. Zhou X et al. Differentiation and persistence of memory CD8(+) T cells depend on T cell factor 1. *Immunity* 33, 229–240 (2010). [PubMed: 20727791]
15. Cui W, Liu Y, Weinstein JS, Craft J & Kaech SM An interleukin-21-interleukin-10-STAT3 pathway is critical for functional maturation of memory CD8+ T cells. *Immunity* 35, 792–805 (2011). [PubMed: 22118527]
16. Ji Y et al. Repression of the DNA-binding inhibitor Id3 by Blimp-1 limits the formation of memory CD8+ T cells. *Nature immunology* 12, 1230–1237 (2011). [PubMed: 22057288]
17. Gattinoni L et al. A human memory T cell subset with stem cell-like properties. *Nature medicine* 17, 1290–1297 (2011).
18. Bender TP, Kremer CS, Kraus M, Buch T & Rajewsky K Critical functions for c-Myb at three checkpoints during thymocyte development. *Nature immunology* 5, 721–729 (2004). [PubMed: 15195090]

19. Dias S et al. Effector Regulatory T Cell Differentiation and Immune Homeostasis Depend on the Transcription Factor Myb. *Immunity* 46, 78–91 (2017). [PubMed: 28099866]
20. Ramsay RG & Gonda TJ MYB function in normal and cancer cells. *Nature reviews. Cancer* 8, 523–534 (2008). [PubMed: 18574464]
21. Greig KT, Carotta S & Nutt SL Critical roles for c-Myb in hematopoietic progenitor cells. *Seminars in immunology* 20, 247–256 (2008). [PubMed: 18585056]
22. Ji Y et al. Identification of the genomic insertion site of Pmel-1 TCR alpha and beta transgenes by next-generation sequencing. *PLoS one* 9, e96650 (2014). [PubMed: 24827921]
23. Seibler J et al. Rapid generation of inducible mouse mutants. *Nucleic acids research* 31, e12 (2003). [PubMed: 12582257]
24. Yuan J, Crittenden RB & Bender TP c-Myb promotes the survival of CD4+CD8+ double-positive thymocytes through upregulation of Bcl-xL. *J Immunol* 184, 2793–2804 (2010). [PubMed: 20142358]
25. Jenkins MK & Moon JJ The role of naive T cell precursor frequency and recruitment in dictating immune response magnitude. *J Immunol* 188, 4135–4140 (2012). [PubMed: 22517866]
26. Appay V, van Lier RA, Sallusto F & Roederer M Phenotype and function of human T lymphocyte subsets: consensus and issues. *Cytometry A* 73, 975–983 (2008). [PubMed: 18785267]
27. van der Windt GJ et al. Mitochondrial respiratory capacity is a critical regulator of CD8+ T cell memory development. *Immunity* 36, 68–78 (2012). [PubMed: 22206904]
28. Zhao L et al. Integrated genome-wide chromatin occupancy and expression analyses identify key myeloid pro-differentiation transcription factors repressed by Myb. *Nucleic acids research* 39, 4664–4679 (2011). [PubMed: 21317192]
29. Taylor D, Badiani P & Weston K A dominant interfering Myb mutant causes apoptosis in T cells. *Genes & development* 10, 2732–2744 (1996). [PubMed: 8946914]
30. Salomoni P, Perrotti D, Martinez R, Franceschi C & Calabretta B Resistance to apoptosis in CTK-2 cells constitutively expressing c-Myb is associated with induction of BCL-2 expression and Myb-dependent regulation of bcl-2 promoter activity. *Proceedings of the National Academy of Sciences of the United States of America* 94, 3296–3301 (1997). [PubMed: 9096387]
31. Omilusik KD et al. Transcriptional repressor ZEB2 promotes terminal differentiation of CD8+ effector and memory T cell populations during infection. *The Journal of experimental medicine* 212, 2027–2039 (2015). [PubMed: 26503445]
32. Dominguez CX et al. The transcription factors ZEB2 and T-bet cooperate to program cytotoxic T cell terminal differentiation in response to LCMV viral infection. *The Journal of experimental medicine* 212, 2041–2056 (2015). [PubMed: 26503446]
33. Boudousquie C et al. Differences in the transduction of canonical Wnt signals demarcate effector and memory CD8 T cells with distinct recall proliferation capacity. *J Immunol* 193, 2784–2791 (2014). [PubMed: 25127860]
34. Sandberg ML et al. c-Myb and p300 regulate hematopoietic stem cell proliferation and differentiation. *Developmental cell* 8, 153–166 (2005). [PubMed: 15691758]
35. Gattinoni L et al. Acquisition of full effector function in vitro paradoxically impairs the in vivo antitumor efficacy of adoptively transferred CD8+ T cells. *The Journal of clinical investigation* 115, 1616–1626 (2005). [PubMed: 15931392]
36. Wirth TC et al. Repetitive antigen stimulation induces stepwise transcriptome diversification but preserves a core signature of memory CD8(+) T cell differentiation. *Immunity* 33, 128–140. [PubMed: 20619696]
37. Klebanoff CA et al. Determinants of successful CD8+ T-cell adoptive immunotherapy for large established tumors in mice. *Clinical cancer research : an official journal of the American Association for Cancer Research* 17, 5343–5352 (2011). [PubMed: 21737507]
38. Chen Z et al. miR-150 Regulates Memory CD8 T Cell Differentiation via c-Myb. *Cell reports* 20, 2584–2597 (2017). [PubMed: 28903040]
39. Im SJ et al. Defining CD8+ T cells that provide the proliferative burst after PD-1 therapy. *Nature* 537, 417–421 (2016). [PubMed: 27501248]
40. Wu T et al. The TCF1-Bcl6 axis counteracts type I interferon to repress exhaustion and maintain T cell stemness. *Sci Immunol* 1 (2016).

41. Utzschneider DT et al. T Cell Factor 1-Expressing Memory-like CD8(+) T Cells Sustain the Immune Response to Chronic Viral Infections. *Immunity* 45, 415–427 (2016). [PubMed: 27533016]
42. Brummelman J et al. High-dimensional single cell analysis identifies stem-like cytotoxic CD8(+) T cells infiltrating human tumors. *J Exp Med* 215, 2520–2535 (2018). [PubMed: 30154266]
43. Mizuguchi G et al. c-Myb repression of c-erbB-2 transcription by direct binding to the c-erbB-2 promoter. *The Journal of biological chemistry* 270, 9384–9389 (1995). [PubMed: 7721862]
44. Reddy MA et al. Opposing actions of c-ets/PU.1 and c-myb protooncogene products in regulating the macrophage-specific promoters of the human and mouse colony-stimulating factor-1 receptor (c-fms) genes. *The Journal of experimental medicine* 180, 2309–2319 (1994). [PubMed: 7964503]
45. Peng S, Lalani S, Leavenworth JW, Ho IC & Pauza ME c-Maf interacts with c-Myb to down-regulate Bcl-2 expression and increase apoptosis in peripheral CD4 cells. *European journal of immunology* 37, 2868–2880 (2007). [PubMed: 17823980]
46. Dash AB, Orrico FC & Ness SA The EVES motif mediates both intermolecular and intramolecular regulation of c-Myb. *Genes & development* 10, 1858–1869 (1996). [PubMed: 8756344]
47. Yang J et al. Identification of p100 as a coactivator for STAT6 that bridges STAT6 with RNA polymerase II. *The EMBO journal* 21, 4950–4958 (2002). [PubMed: 12234934]
48. Crompton JG, Sukumar M & Restifo NP Uncoupling T-cell expansion from effector differentiation in cell-based immunotherapy. *Immunological reviews* 257, 264–276 (2014). [PubMed: 24329803]
49. Gattinoni L et al. Wnt signaling arrests effector T cell differentiation and generates CD8+ memory stem cells. *Nature medicine* 15, 808–813 (2009).
50. Sabatino M et al. Generation of clinical-grade CD19-specific CAR-modified CD8+ memory stem cells for the treatment of human B-cell malignancies. *Blood* 128, 519–528 (2016). [PubMed: 27226436]

METHODS-ONLY REFERENCES

51. Yang Q et al. TCF-1 upregulation identifies early innate lymphoid progenitors in the bone marrow. *Nature immunology* 16, 1044–1050 (2015). [PubMed: 26280998]
52. Eil R et al. Ionic immune suppression within the tumour microenvironment limits T cell effector function. *Nature* 537, 539–543 (2016). [PubMed: 27626381]
53. Kim D et al. TopHat2: accurate alignment of transcriptomes in the presence of insertions, deletions and gene fusions. *Genome Biol* 14, R36 (2013). [PubMed: 23618408]
54. Love MI, Huber W & Anders S Moderated estimation of fold change and dispersion for RNA-seq data with DESeq2. *Genome Biol* 15, 550 (2014). [PubMed: 25516281]
55. Gu Z, Eils R & Schlesner M Complex heatmaps reveal patterns and correlations in multidimensional genomic data. *Bioinformatics* 32, 2847–2849 (2016). [PubMed: 27207943]
56. Subramanian A et al. Gene set enrichment analysis: a knowledge-based approach for interpreting genome-wide expression profiles. *Proceedings of the National Academy of Sciences of the United States of America* 102, 15545–15550 (2005). [PubMed: 16199517]
57. Roychoudhuri R et al. Transcriptional profiles reveal a stepwise developmental program of memory CD8(+) T cell differentiation. *Vaccine* 33, 914–923 (2015). [PubMed: 25446821]

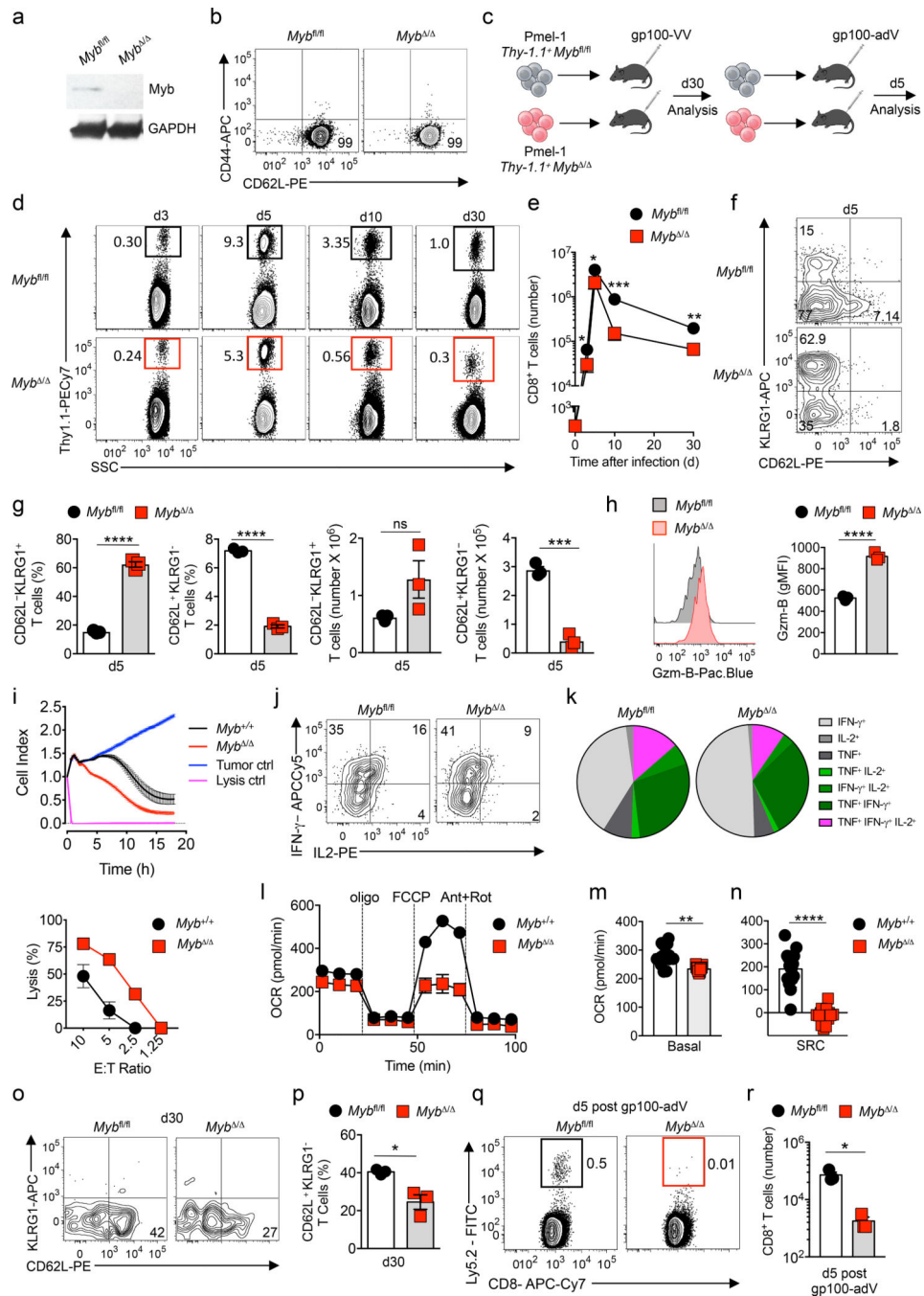


Figure 1. c-Myb promotes the formation stem cell-like T_{CM} cells by restraining terminal differentiation.

(a) Immunoblot showing c-Myb in naïve CD8⁺ T cells from pmel-1 *Myb^{fl/fl} Cre-ERT2* mice 5d after i.p. treatment with tamoxifen or vehicle. GAPDH served as control. (b) Flow cytometry of pmel-1 *Myb^{fl/fl}* and *Myb^{Δ/Δ}* CD8⁺ T cells after naïve T cell enrichment. (c) Experimental design testing c-Myb impact on pmel-1 CD8⁺ T cell primary and secondary immune responses. gp100-VV, vaccinia virus encoding human gp100; gp100-adV, adenovirus type 2 encoding human gp-100. (d,e) Flow cytometry of splenic CD8⁺ T cells

(d) and numbers of pmel-1 T cells **(e)** after transfer of 10^5 pmel-1 Thy1.1 *Myb^{fl/fl}* or pmel-1 Thy1.1 *Myb^{-/-}* CD8⁺ T cells into wild-type mice infected with gp100-VV, assessed 0–30 d after infection ($n = 3$ mice per group per time point). **(f)** Flow cytometry of pmel-1 T cells 5d after transfer as in **d,e**. **(g)** Percentages (left) and numbers (right) of CD62L⁻ KLRG1⁺ and CD62L⁺ KLRG1⁻ pmel-1 T cells 5d after transfer as in **d,e**. **(h)** Flow cytometry (left) and geometric Mean Fluorescence Intensity (right) of pmel-1 T cells 5d after transfer as described in **d**. **(i)** Cell index (top) and percentage of lysis (bottom) of B16-hgp100 melanoma after co-culture with pmel-1 *Myb^{+/+}* or pmel-1 *Myb^{-/-}* CD8⁺ T cells ($n = 6$ technical replicates) **(j,k)** Intracellular cytokine staining **(j)** and combinatorial cytokine production **(k)** by pmel-1 T cells 5d after transfer as in **d,e**. **(l)** Oxygen consumption rate (OCR) of pmel-1 *Myb^{+/+}* and pmel-1 *Myb^{-/-}* CD8⁺ T cells activated *in vitro* with anti-CD3 and anti-CD28 antibodies in the presence of IL-2. Data are shown under basal condition and in response to the indicated molecules ($n = 5$ technical replicates). FCCP, Carbonyl cyanide 4-(trifluoromethoxy)phenylhydrazone; Ant, Antimycin; Rot, Rotenone. **(m, n)** Basal OCR **(m)** and SRC **(n)** of pmel-1 T cells generated as in **l** ($n = 15$ technical replicates; 5 replicates x 3 time points). SRC, spare respiratory capacity. **(o)** Flow cytometry of pmel-1 T cells in the lymph nodes 30d after transfer as in **d,e**. **(p)** Percentage of KLRG1⁻CD62L⁺ pmel-1 T cells in the lymph nodes 30d after transfer as in **d,e**. **(q,r)** Flow cytometry of splenocytes **(q)** and numbers of splenic pmel-1 T cells **(r)** 5d after the transfer of 5×10^4 pmel-1 Ly5.2 *Myb^{fl/fl}* and pmel-1 Ly5.2 *Myb^{-/-}* primary memory CD8⁺ T cells followed by secondary infection with gp100-adV ($n = 3$). Data are representative of at least two independent experiments. Data are shown after gating on live CD8⁺ **(b, d)**, CD8⁺ Thy1.1⁺ cells **(f, h, j, o)** and CD8⁺ Ly5.2⁺ **(q)**. Data in **e, g, h, j, i, l, m, n, p** and **r** are shown as mean \pm s.e.m.; shapes represent individual mouse **(g, h, p** and **r)** or technical replicates **(i, m, n)**. * = $P < 0.05$, ** = $P < 0.01$, *** = $P < 0.001$ and **** = $P < 0.0001$, ns = non-significant (unpaired two-tailed Student's *t*-test).

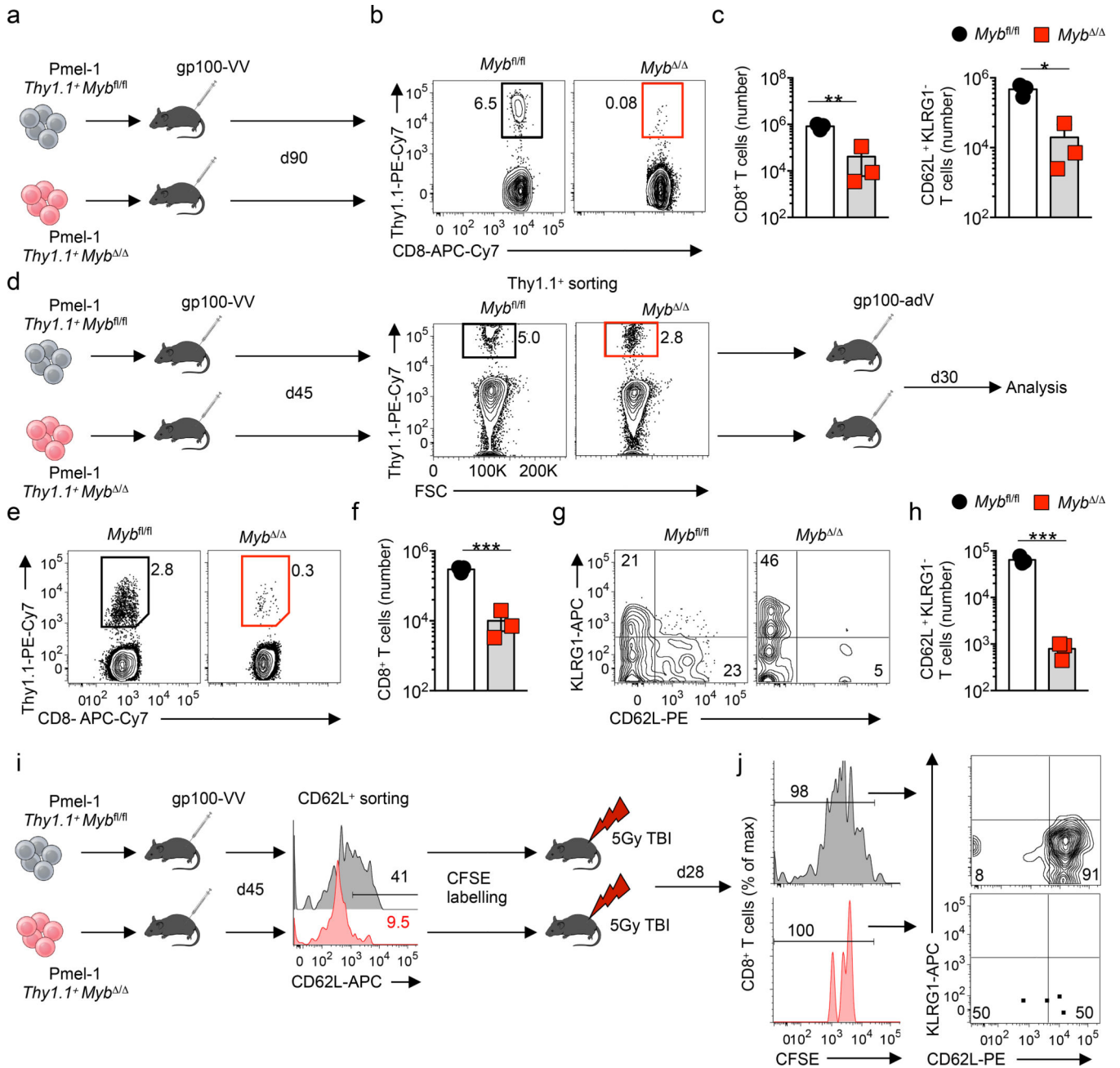


Figure 2. c-Myb is indispensable for CD8⁺ T cell stemness.

(a) Experimental design assessing c-Myb function in long-term memory. (b) Flow cytometry of splenic CD8⁺ T cells after transfer of 3×10^5 pmel-1 *Thy1.1 Myb^{fl/fl}* or pmel-1 *Thy1.1 Myb^{Δ/Δ}* CD8⁺ T cells into wild-type mice infected with gp100-VV, assessed 90d after infection ($n = 3$ mice per group). (c) Numbers of total (left) and CD62L⁺ KLRG1⁻ (right) pmel-1 T cells after transfer as in b. (d) Experimental design testing c-Myb impact on secondary memory. Middle, flow cytometry exemplifying Thy1.1⁺ T cell frequencies 45d after transfer as in b. (e, f) Flow cytometry of splenocytes (e) and numbers of splenic pmel-1 Thy1.1 CD8⁺ T cells (f) after transfer of 5×10^4 primary memory pmel-1 *Thy1.1 Myb^{fl/fl}* or

pmel-1 Thy1.1 *Myb*^Δ CD8⁺ T cells, assessed 30d after gp100-adV infection ($n = 3$ mice per group). (g) Flow cytometry of splenic pmel-1 T cells 30d after transfer as in e,f. (h) Numbers of splenic CD62L⁺ KLRG1⁻ pmel-1 T cells obtained as in g. (i) Experimental design evaluating self-renewal of stem cell-like T_{CM} cells. Middle, flow cytometry exemplifying the sorting strategy for isolation of CD62L⁺ pmel-1 memory T cells from spleens and lymph nodes 45d after transfer of 10⁶ pmel-1 Thy1.1 *Myb*^{fl/fl} or pmel-1 Thy1.1 *Myb*^Δ CD8⁺ T cells into wild-type mice infected with gp100-VV. (j) Flow cytometry of pmel-1 Thy1.1 CD8⁺ T cells 28d after transfer of 10⁵ CFSE-labeled CD62L⁺ pmel-1 Thy1.1 *Myb*^{fl/fl} or pmel-1 Thy1.1 *Myb*^Δ CD8⁺ T cells into sub-lethally irradiated mice ($n = 2$ mice per group, data shown after concatenating). Data are shown after gating on live (e) live, CD8⁺ (b, d) and live, CD8⁺ Thy1.1⁺ cells (g, j). Data in c, f, h are shown as mean ± s.e.m.; shapes represent individual mice (c, f, h). * = $P < 0.05$, ** = $P < 0.01$ and *** = $P < 0.001$ (unpaired two-tailed Student's *t*-test).

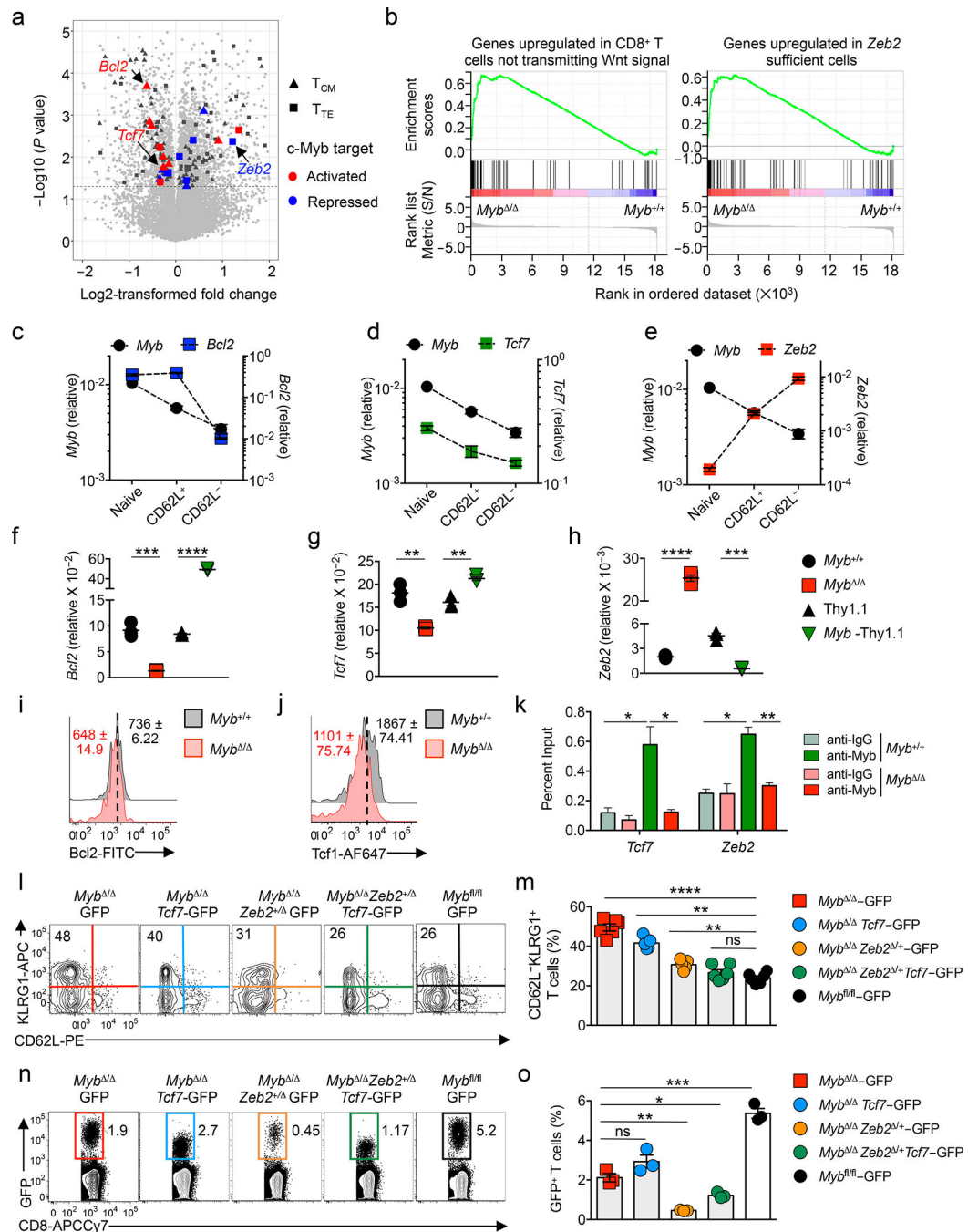


Figure 3. c-Myb enhances CD8⁺ T cell stemness by regulating *Tcf7*, *Bcl2*, and *Zeb2* expression (a) Volcano plot showing changes in gene expression between pmel-1 *Myb*^{+/+} and pmel-1 *Myb*^{-/-} T cells. Gene expression was evaluated by RNA-seq of pmel-1 KLRG1⁺CD62L⁻ T cells isolated 5 days after transfer of 3 × 10⁵ pmel-1 Thy1.1 *Myb*^{+/+} and pmel-1 Thy1.1 *Myb*^{-/-} CD8⁺ T cells into wild-type mice infected with gp100-VV (*n* = 3, each from 2 pooled mice per group). Triangles and squares represent genes enriched in central memory (T_{CM}) and terminal effector (T_{TE}) T cells⁵⁷, respectively. Red and blue represent genes activated and repressed by c-Myb in promyelocytes, respectively²⁸. (b) Gene Set

Enrichment Assay showing positive enrichment of genes upregulated in cells lacking Wnt signaling³³ (left) and in *Zeb2*-sufficient cells³² (panel) in pmel-1 *Myb*^{-/-} T cells obtained as in **a**. (**c–e**). Quantitative RT-PCR of *Bcl2* (**c**), *Tcf7* (**d**) and *Zeb2* (**e**) mRNA in comparison to *Myb* in naïve, CD62L⁺ and CD62L⁻ pmel-1 T cells sorted 5d after transfer of 10⁵ pmel-1 *Myb*^{+/+} CD8⁺ T cells as in **a**. Results are relative to *Rpl13* (*Bcl2*, *Tcf7* and *Zeb2*) or *Actb* (*Myb*) ($n = 3$ technical replicates). (**f–h**) Quantitative RT-PCR of *Bcl2* (**f**), *Tcf7* (**g**) and *Zeb2* (**h**) mRNA in pmel-1 CD62L⁺ T cells sorted 5d after transfer of 10⁵ pmel-1 Thy1.1 *Myb*^{+/+}, pmel-1 Thy1.1 *Myb*^{-/-}, pmel-1 Thy1.2⁺ engineered with *Myb*-Thy1.1 or Thy1.1 as in **a**. Results are relative to *Rpl13* ($n = 3$ technical replicates). (**i,j**) Flow cytometry of pmel-1 T cells 5d after transfer of 10⁵ pmel-1 Thy1.1 *Myb*^{+/+}, pmel-1 Thy1.1 *Myb*^{-/-} as in **a**. Numbers indicate geometric Mean Fluorescence Intensity \pm s.e.m. ($n = 3$ mice per group) (**k**) ChIP-qPCR of *in vitro* activated pmel-1 *Myb*^{+/+} or pmel-1 *Myb*^{-/-} CD8⁺ T cells. Chromatin was precipitated with anti-c-Myb or anti-IgG antibodies and amplified with primers specific to *Tcf7* enhancer and *Zeb2* promoter regions ($n = 3$ technical replicates). **l, n** Flow cytometry of splenic pmel-1 T cells (**l**) and CD8⁺ T cells (**n**) after transfer of 10⁵ pmel-1 *Myb*^{fl/fl}, pmel-1 *Myb*^{-/-} or pmel-1 *Myb*^{-/-} *Zeb2*^{+/-} CD8⁺ T cells transduced with pMI-GFP or pMI-GFP-*Tcf7* 10 d after transfer into wild-type mice infected with gp100-VV. **m, o** Percentage of KLRG1⁺CD62L⁻GFP⁺CD8⁺ T cells (**m**) and CD8⁺ GFP⁺ T cells (**o**) 10 d after transfer as in **l**. Data are representative of two independent experiments. Data are shown after gating on live CD8⁺ Thy1.1⁺ cells (**i, j**), live CD8⁺ GFP⁺ cells (**l**) or live CD8⁺ cells (**n**). Data in **c–h, k,m,o** are mean \pm s.e.m.; each symbol represents an individual mouse (**m, o**) or technical replicate (**c–h, k**). **m**, merged data from two independent experiments. * $P < 0.05$, ** $P < 0.01$, *** $P < 0.001$ and **** $P < 0.0001$ (unpaired two-tailed Student's *t*-test).

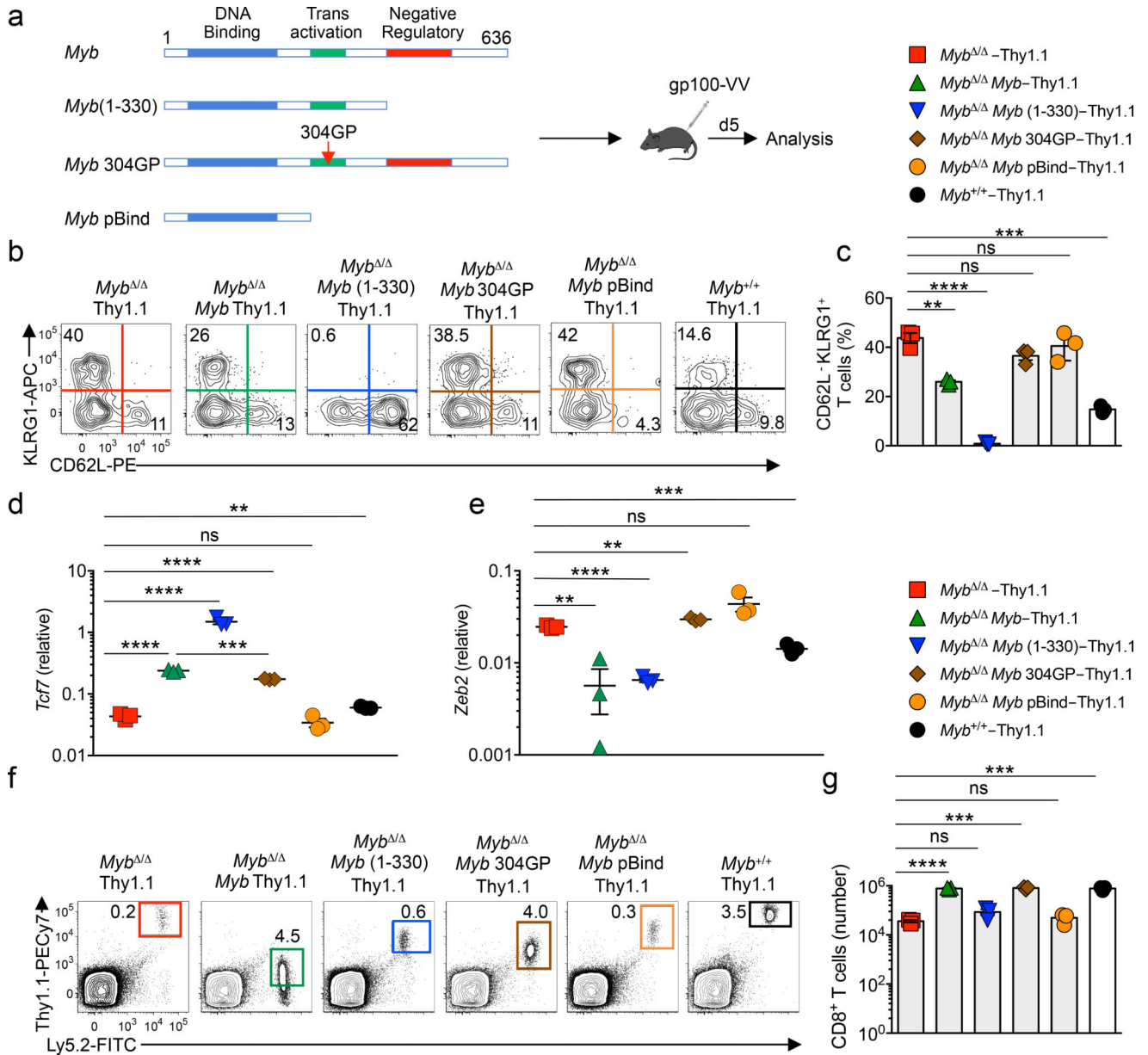


Figure 4. Distinct functions of c-Myb domains in the regulation of CD8⁺ T cell differentiation and survival.

(a) Truncated and mutated versions of c-Myb employed for complementation studies. (b) Flow cytometry of splenic pmel-1 Thy1.1 CD8⁺ T cells 5d after transfer of 10⁵ pmel-1 *Myb*^{-/-} CD8⁺ T cells, transduced with MSGV-Thy1.1 encoding wild-type or mutated c-Myb forms, into Ly5.1 mice infected with gp100-VV. pmel-1 *Myb*^{+/+} and pmel-1 *Myb*^{-/-} CD8⁺ T cells transduced with Thy1.1 served as control (*n* = 3 mice per group). (c) Percentage of KLRG1⁺ CD62L⁻ pmel-1 T cells 5d after transfer as in b. Quantitative RT-PCR of *Tcf7* (d) and *Zeb2* (e) mRNA in pmel-1 T cells sorted 5d after transfer as in b. Results are relative to *Rpl13* (*n* = 3 technical replicates). (f) Flow cytometry of CD8⁺ T cells 5d after transfer as described in b. (g) Percentage of splenic CD8⁺ Thy1.1⁺ T cells 5d after transfer as described in b. Data are representative of at least two independent experiments. Data are shown after

gating on live CD8⁺ Thy1.1⁺ cells (**b**), and live CD8⁺ cells (**f**). Data in **c–e**, and **g** are shown as the mean \pm s.e.m.; shapes represent individual mice (**c** and **g**) or technical replicates (**d,e**). **= $P < 0.01$, ***= $P < 0.001$ and ****= $P < 0.0001$; ns, non-significant (unpaired two-tailed Student's *t*-test).

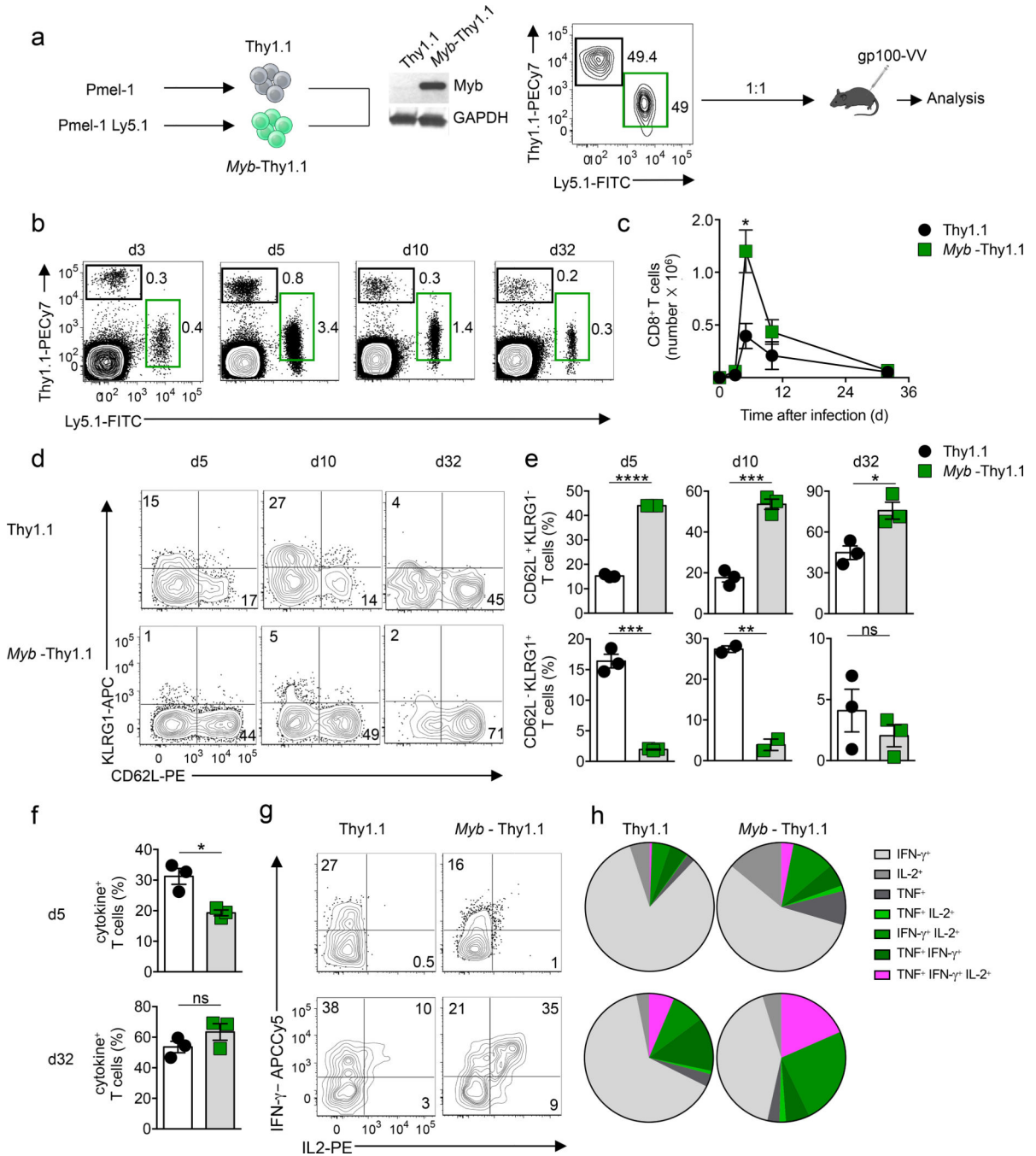


Figure 5. *Myb* overexpression enhances CD8⁺ T cell memory and polyfunctionality.

(a) Experimental design evaluating the impact of *Myb* overexpression in CD8⁺ T cell memory formation. Left, immunoblot of c-Myb in Thy1.1 and *Myb*-Thy1.1 overexpressing cells. Right, flow cytometry of the 1:1 mixture of Thy1.1 and *Myb*-Thy1.1 CD8⁺ T cells before transfer into mice. gp100-VV, vaccinia virus encoding human gp100 (b,c) Flow cytometry of splenic CD8⁺ T cells (b) and numbers of pmel-1 T cells (c) after co-transfer of 5×10^4 pmel-1-Thy1.1 and 5×10^4 pmel-1 Ly5.1 *Myb*-Thy1.1 CD8⁺ T cells into wild-type mice infected with gp100-VV. Assessed 0–32d after transfer ($n = 3$ mice per group per time

point). **(d)** Flow cytometry analysis of splenic pmel-1 T cells after transfer as in **b,c**. **(e)** Percentage of KLRG1⁻CD62L⁺ (upper panel) and KLRG1⁺ CD62L⁻ (lower panel) splenic pmel-1 T cells after transfer as in **b,c**. **(f)** Percentage of cytokine producing pmel-1 T cells after transfer as described in **b,c**. **(g, h)** Intracellular cytokine staining **(g)** and combinatorial cytokine production **(h)** by splenic pmel-1 T cells 5d after transfer as in **b,c**. Data are representative of two independent experiments. Data are shown after gating on live CD8⁺ cells **(b)**, and live CD8⁺ Thy1.1⁺ **(d, g)**. Data in **c, e**, and **f** are shown as the mean \pm s.e.m.; shapes represent individual mice. * = $P < 0.05$, ** = $P < 0.01$, *** = $P < 0.001$ and **** = $P < 0.0001$ (unpaired two-tailed Student's *t*-test).

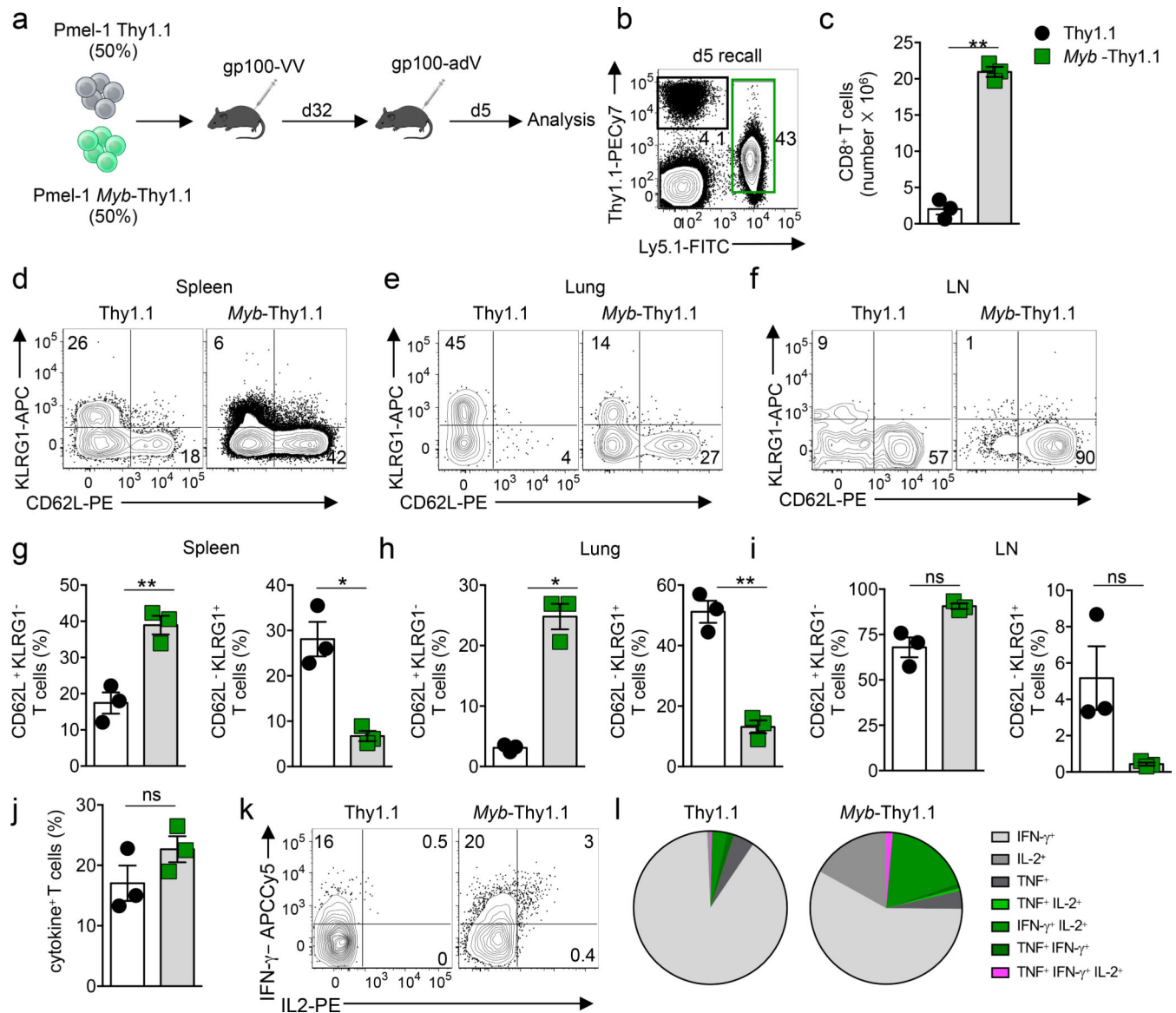


Figure 6. *Myb* overexpression enhances CD8⁺ T recall responses.

(a) Experimental design testing the impact of *Myb* overexpression on CD8⁺ T cell secondary responses. gp100-VV, vaccinia virus encoding human gp100; gp100-adV, adenovirus type 2 encoding gp-100. (b, c) Flow cytometry of splenic CD8⁺ T cells (b) and numbers of pmel-1 CD8⁺ T cells (c) after co-transfer of 5×10^4 pmel-1-Thy1.1 and 5×10^4 pmel-1 Ly5.1 *Myb*-Thy1.1 CD8⁺ T cells into wild-type mice infected with gp100-VV, assessed 5d after secondary infection with gp100-adV ($n = 3$ mice per group). (d–f) Flow cytometry of pmel-1 T cells in the spleen (d), lungs (e) and lymph nodes (f) 5d after secondary infection as in b,c. (g–i) Percentage of KLRG1⁻CD62L⁺ and KLRG1⁺CD62L⁻ pmel-1 T cells in the spleen (g), lungs (h) and lymph nodes (i) 5d after secondary infection as in b,c. (j) Percentage of cytokine⁺ splenic pmel-1 T cells 5d after secondary infection as in b,c. (k, l) Intracellular cytokine staining (k) and combinatorial cytokine production (l) by splenic pmel-1 T cells 5d after secondary infection as in b,c. Data are representative of two

independent experiments. Data are shown after gating on live CD8⁺ cells (**b**), and live CD8⁺ Thy1.1⁺ (**d–f**, **k**). Data in **c**, and **g–j**, are shown as the mean \pm s.e.m.; shapes represent individual mice. * = $P < 0.05$, ** = $P < 0.01$; ns, non-significant (unpaired two-tailed Student's *t*-test).

Author Manuscript

Author Manuscript

Author Manuscript

Author Manuscript

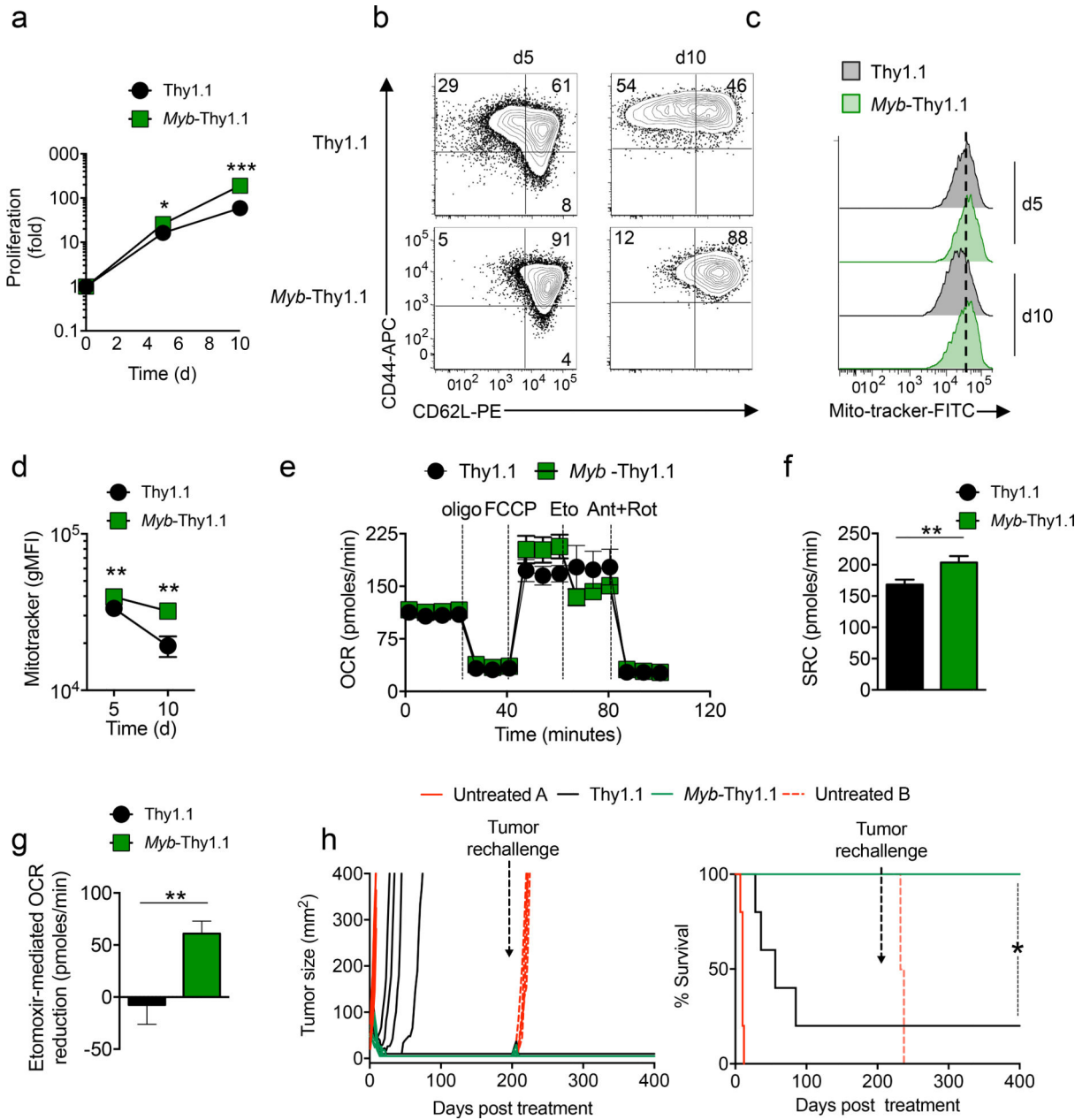


Figure 7. Enforced expression of *Myb* enhances CD8⁺ T cell antitumor immunity.

(a) Fold expansion of pmel-1 CD8⁺ T cells transduced with Thy1.1 or *Myb*-Thy1.1 cells after priming with anti-CD3 anti-CD28 antibodies and re-stimulation with the same antibodies 5d later. Cells were grown in the presence of IL-2 throughout the culture ($n = 3$ independent experiments). (b, c) Flow cytometry of pmel-1 T cells transduced with Thy1.1 or *Myb*-Thy1.1 generated as described in a. (d) geometric Mean Fluorescence Intensity (gMFI) of mitotracker staining in pmel-1 T cells generated as in a. ($n = 3$ technical replicates) (e) Oxygen consumption rate (OCR) of pmel-1 T cells generated as in a., assessed on 10d. Data are shown under basal culture conditions and in response to the indicated molecules ($n = 12$ technical replicates). FCCP, Carbonyl cyanide 4-

(trifluoromethoxy)phenylhydrazine; Ant, Antimycin; Eto, Etomoxir; Rot, Rotenone. **(e,f)** Spare respiratory capacity (SRC) **(g)** and reduction of OCR after Eto administration in pmel-1 T cells generated as in **a.**, assessed on 10d ($n = 36$ technical replicates; 12 replicates \times 3 time points) **(i)** Tumor curve (left panel) and survival (right panel) of wild-type mice bearing subcutaneous hgp100⁺ B16 melanoma cells after transfer of 5×10^6 pmel-1 T cells generated as in **a** in conjunction with gp100-VV and IL-2 ($n = 5$ mice per group). Solid and dashed red curve denotes tumor challenged mice that received no T cell transfer. On 206d post-T cell transfer, mice were re-challenged with 2.5×10^5 hgp100⁺ B16 melanoma. Data are representative of two independent experiments. Tumor re-challenge after 200d was performed in an individual experiment. Data are shown after gating on live CD8⁺ cells **(b, c)** Data in **a, d–g** are shown as the mean \pm s.e.m.; each tumor curve represents an individual mouse $* = P < 0.05$, $*** = P < 0.001$ (**a**, unpaired two-tailed Student's *t*-test; **h**, a Log-rank (Mantel-Cox) Test).